Model Based Virtual Prototyping for Hydraulic Passive Engine Mount with an Emphasis on Inertia Track

by

Amirhossein Sarafrazian

B.Sc., Azad University of Tehran, 2001

Thesis Submitted in Partial Fulfillment of the
Requirements for the Degree of
Master of Applied Science

in the
School of Engineering Science
Faculty of Applied Sciences

© Amirhossein Sarafrazian 2013

SIMON FRASER UNIVERSITY

Spring 2013

All rights reserved.
However, in accordance with the *Copyright Act of Canada*, this work may be reproduced, without authorization, under the conditions for "Fair Dealing." Therefore, limited reproduction of this work for the purposes of private study, research, criticism, review and news reporting is likely to be in accordance with the law, particularly if cited appropriately.

Approval

Name: **Amirhossein Sarafrazian**

Degree: **Master of Applied Science**

Title of Thesis: ***Model Based Virtual Prototyping for Hydraulic Passive Engine Mount with an Emphasis on Inertia Track***

Examining Committee: **Chair:** Dr. Gary Wang
Professor

Dr. Farid Golnaraghi
Senior Supervisor
Professor _____

Dr. Siamak Arzanpour
Senior Supervisor
Assistant Professor _____

Dr. Mehrdad Moallem
Supervisor
Professor _____

Dr. Krishna Vijayaraghavan
Internal Examiner
Assistant Professor _____

Date Defended/Approved: March 25, 2013

Partial Copyright Licence

The author, whose copyright is declared on the title page of this work, has granted to Simon Fraser University the right to lend this thesis, project or extended essay to users of the Simon Fraser University Library, and to make partial or single copies only for such users or in response to a request from the library of any other university, or other educational institution, on its own behalf or for one of its users.

The author has further granted permission to Simon Fraser University to keep or make a digital copy for use in its circulating collection (currently available to the public at the "Institutional Repository" link of the SFU Library website (www.lib.sfu.ca) at http://summit/sfu.ca and, without changing the content, to translate the thesis/project or extended essays, if technically possible, to any medium or format for the purpose of preservation of the digital work.

The author has further agreed that permission for multiple copying of this work for scholarly purposes may be granted by either the author or the Dean of Graduate Studies.

It is understood that copying or publication of this work for financial gain shall not be allowed without the author's written permission.

Permission for public performance, or limited permission for private scholarly use, of any multimedia materials forming part of this work, may have been granted by the author. This information may be found on the separately catalogued multimedia material and in the signed Partial Copyright Licence.

While licensing SFU to permit the above uses, the author retains copyright in the thesis, project or extended essays, including the right to change the work for subsequent purposes, including editing and publishing the work in whole or in part, and licensing other parties, as the author may desire.

The original Partial Copyright Licence attesting to these terms, and signed by this author, may be found in the original bound copy of this work, retained in the Simon Fraser University Archive.

Simon Fraser University Library
Burnaby, British Columbia, Canada

revised Fall 2011

Abstract

This thesis presents modifications of the hydraulic engine mount prediction program, HEMPP, which is currently used in the automotive industry to match the mount to the experimental results by predicting the dynamic stiffness and phase angle of the mount. The main focuses of this thesis are the identification, simulation, and verification of a new model for measuring pressure drop fluctuations of periodically fluctuating flow inside the inertia track of the hydraulic engine mount and its resistance. Moreover, to achieve a new model for resistance, the friction factor of fluid under frequency excitation, which is a main cause of discrepancies between simulation and experimental results, has been investigated. Two major findings were explored in previous studies have been used in this research: First, the friction coefficient in oscillatory and reciprocating flow inside a finite length of pipe depends on the kinetic Reynolds number and the dimensionless oscillation amplitude of the fluid; and second, the linear model and the equations of the typical engine mount have been significantly examined. An extensive set of experiments have been conducted using two test apparatuses to provide numerical data. One examined the effect of a pipe's geometrical parameters such as cross sectional area and roughness on the frequency response of the pressure difference between the entrance and exit of the finite length pipe. The second test apparatus has been employed to validate the equations of pressure drop in the inertia track of an engine mount. Finally, a new model of resistance was implemented in the old version of the prediction program, showing that the frequency responses of dynamic stiffness simulated by this modified prediction program agreed with the experimental results. This new model could be employed to predict the hydraulic engine mount performance in order to create products confirming more closely to customer needs.

Keywords: Engine Mount; Fluid, Resistance; HEMPP; Dynamic Stiffness;

Acknowledgements

I would like to express my most sincere gratitude to my supervisors Dr. Golnaraghi and Dr. Arzanpour for their input and support with this project. Without their forceful encouragements, constructive criticisms and enthusiastic guidance, completion of this work would not have been possible. Their guidance enabled me to follow the right direction to solve the problem.

Gratefully, Dr. Golnaraghi accepted me to work as a graduate student in his team and provided me the valuable opportunity to return to school after 10 years, which has had a great impact on my life. I would like to recognize Dr. Arzanpour's extensive advice and many ideas in setting up the tests and handling the project. He provided tremendous help and was always available for support. I also wanted to thank Dr. Behfarshad; his expertise in mechanics of fluid was the great help to solve the project. Special thanks are extended to Dr. Moallem and Dr. Vijayaraghavan for reading my thesis, their providing input, and attending in my defence as the committee supervisor and the internal examiner, respectively. I would like to extend my gratefulness to Dr. Wang for his time and energy as my session defence chair.

Last but not least, I am extremely grateful to my beloved family, my parents Mohsen and Vahideh and my wife, Shabnam for their pure love, sacrifices, prayers and emotional supports through my life. This work would not be possible without their encouragements. I also wanted to extend my appreciation to my in-laws, Parviz and Behnaz and my brothers and sister Maham, Amirali and Nasim for their love and support.

Table of Contents

List of Figures

Nomenclature

A_0	dimensionless amplitude of oscillation
A_p	effective piston area of engine mount
b_i	viscous friction in the pipe
b_r	damping of main rubber of upper chamber
c	damping coefficient in mass spring system
c_1, c_2	compliance of upper and lower chamber
C_f	Blasius friction factor
D	diameter of pipe
D_h	hydraulic diameter
f	friction factor
f_D	Darcy friction factor
F_1, F_2	hydraulic forces induced in the entrance and exit of inertia track
F_T	force transmitted to the basis
g	gravity
h_f	head loss
I_i	inertia of inertia track
k	stiffness of spring in mass spring system, entrance loss
K_1, K_2	stiffness of upper and lower chamber
K_d	dynamic stiffness of engine mount
K_r	stiffness of main rubber of upper chamber
L	length of pipe
M_i	mass passes through inertia track

m	mass of mass spring system
P_1,P_2	pressure of upper and lower chamber
Q_i,Q_d	flow passing through inertia track and decoupler
r	frequency ratio, radius
R_i	resistance of inertia track
R_l	resistance of inertia track in laminar flow
R_t	resistance of inertia track in turbulent flow
t	time
v, u, w	speed of fluid in different directions
x	mass displacement in mass spring system
X_e	engine displacement
y_b	amplitude of base oscillation

Greek symbols

α	Womersley number
ω_b	frequency of base oscillation
ζ	damping ratio
ε	roughness
ω_n	natural frequency
ϕ	phase shift between velocity and externally imposed pressure gradient
τ_w	shear stress of the wall of a pipe

1. Introduction

Isolating passengers of a vehicle from vibrations and noise is a considerable challenge the automotive industry is facing. When the engine of a car is running, regardless of whether the car is moving normally or stopping, vibration and noise disturbances are induced; but when these are absorbed by the vehicle, the passengers enjoy a more comfortable ride. There are two sources of noise during driving: the engine and road conditions. Rotation of shafts and combustion of fuel inside the cylinders of an engine provide high-frequency excitation at low amplitude. Engine speed, number of cylinders, and stroke number are the sources of unbalanced engine vibration [1]. For example, a four-cylinder, four-stroke engine produces a frequency of disturbances in the range of 20 to 200 Hz for engine speeds ranging from 600 to 6000 rpm, while an eight-cylinder engine produces a frequency in the range of 40 to 400 Hz for the same engine speed range [7]. The second reason for vibrations, road conditions, can induce large amplitude disturbance along with low frequency. So the range of frequency disturbance varies from 5 to 400 Hz [1].To absorb these noises and provide a smooth ride, manufacturers use three kinds of engine mount: active, semi-active, and passive. Normally, high amplitudes are induced by engine at idle and low speeds, while at higher speeds, the engine creates lower amplitude. Moreover, amplitude induced by engine vibration is smaller than 0.3 mm at the high frequencies of 50 to 300 Hz and larger than 0.3 mm at frequencies smaller than 50 Hz [1].

An engine mount has frequency and amplitude dependency characteristics and is designed to have different responses to various excitations. To control idle shakes and road-induced excitations, the engine mount must be highly damped and stiff, while for small amplitude vibrations over the higher frequency range caused by the engine, vibration isolation and acoustic comfort are needed. The engine mount therefore has to meet these two necessary but conflicting criteria. Spiekermann et al. [3] demonstrated a simulation and optimization for solving a common vibration isolation problem involving a

rigid body on a compliant mount by using an interactive computer program, ENGSIM. Royston and Singh [4] formulated an analytical framework for the design optimization of a multi-degree of freedom mounting system considering its nonlinear effects and parallel passive design and active control concept.

The two main roles of an ideal engine mount are to isolate the noises induced by operation of the engine, and to prevent engine bounce from the vehicle frame excitation. Moreover, the ideal engine mount should reduce the amplitude of engine vibrations that are transmitted to the body of car and noise amplification caused by the engine. It also should decrease human discomfort and fatigue by isolating the vibrations from the body. In addition, it must prevent large engine-to-chassis relative movement caused by torque reaction force of road bumps shocks [8].Yu et al. [7] performed a comprehensive literature review on all kinds of engine mounts; they show that disturbances inertia force has two components, one is parallel to and one is perpendicular to the crankshaft axis and inertia torque is also parallel to the crankshaft axis.

Nowadays, by improving the automotive technology and industry, car companies are starting to design more luxury vehicles based on the market demands, with higher power and speed and comfort along with lighter bodies and chassis. The new concerns about improving cars result in an increase in the ratio of weight of engine to the weight of car, making the design of more effective engine mounts highly desirable. Different types of engine mounts have been used in the automotive industry such as rubber mounts, passive mounts, semi-active mounts, and active hydraulic engine mounts. Here we introduce all of them considering their functionality and performance. Because the rubber mount was the first mount applied to isolate the cabin from engine disturbances, we start by first introducing that mount.

1.1. Rubber mount

Rubber is widely used in many applications because of its great reversible elastic deformation, and damping and energy absorption characteristics. Rubber (elastomeric) mounts have been used since the 1930s to isolate passengers from engine noises [5].

A rubber mount consists of a bulk rubber that is casted in a metal casing and a mounting rod. To study the attitude of the rubber mounts in noise isolation, Wang et al. [49] predicted the static and dynamic characteristic of the rubber mount; they meshed the subject by PATRAN and finalized computation by ADINA and ABAQUS. They showed that stress on rubber can be measured by using Von Mises strain-stress. Kim et al. [6] investigated the estimation of fatigue life of rubber engine mounts to ensure their durability at different conditions of use. They predicted fatigue damage of natural rubber by using maximum Green-Lagrange strain parameters. Tian et al. [9] evaluated stiffness and damping of a rubber mount as frequency dependent parameters, they studied the transition of the rubber mount stiffness from static to dynamic values by applying least-squares polynomial curve fitting to data obtained from the test. These types of mounts have been designed and used because of their elastic stiffness rate characteristic in all directions. They are also compact, inexpensive and easy to replace; provide more consistent performance; and have a longer life. The dynamic stiffness of rubber mounts at lower frequencies is smaller than its stiffness at higher frequencies of excitation providing better absorption of road noises than of engine noises [10]. Although rubber materials are widely used for controlling structural vibration and sound radiation, their visco-elastic behaviour makes their dynamic properties hard to define. With this characteristic, it would be difficult to design the mount that can satisfy the requirements of noise absorption. Although they show good performance at low frequencies by their high stiffness and damping, they provide poor isolation at higher frequencies. Rubber mounts have been used in vehicles for many years, but by developing the heavier engine and lighter body used in faster cars, especially front wheel drive cars, it is necessary to use mounts with better performance.

1.2. Passive hydraulic engine mount

The passive hydraulic engine mount is the component that has been used in vehicles to tolerate the engine weight, keep it tightly attached to the chassis, as well as prevent the occupants from feeling the vibrations and disturbances of the engine and road conditions by acting as a shock absorber. It was patented by Richard Rasmussen

in 1962 for increasing damping [11]. The passive engine mount is used widely for two reasons: First car manufacturers plan to build smaller cars with lighter bodies and front wheel drive power trains, because of fuel efficiency, requires more complex mounting systems; and second, the mount has dual characteristics. This engine mount has amplitude and frequency dependant characteristics that can significantly reduce low-frequency vibration, isolate high-frequency vibration, and provide consequential damping or stiffness to control the firm body movement of the engine. Different types of passive engine mounts have been created to absorb the disturbances of engines, resulting in tremendous progress in ride comfort and decreased noise levels compared with conventional elastomeric mounts. The passive engine mount contains two chambers, filled with liquid, which are connected by inertia track and decoupler. Bernuchon [12] and Corcoran et al. [13] have shown that the mount can reduce noise level by 5 dB, bringing more comfort to passengers. Various types of passive hydraulic engine mounts are similar in concept but different in details of structural design. Typically, the different types include hydraulic mounts with simple orifices, hydraulic mounts with inertia track and hydraulic mounts with inertia track and decoupler. Although hydraulic mounts with simple orifices and mounts with inertia track have similar characteristics in providing damping at lower frequencies, the mount with inertia track creates more damping than the other type [14]. It can be adjusted to have more damping especially at higher amplitude of excitation used to decrease shock levels. Although these models work well in increasing the damping at low frequencies, at high frequencies they do not perform well in terms of noise isolation. To solve this problem, a decoupler has been added to act as amplitude limited floating piston, which causes the mount to be amplitude-dependent at high frequencies and low displacement. It allows the mount to have the characteristics of the elastomeric mount and induces excellent vibration isolation at larger displacement [7]. At larger amplitude and lower frequencies, the pumping of upper compliance makes the decoupler sit in the bottom of cage and closes the orifices, making the inertia track the only way for liquid to move to the lower compliance. At higher frequencies and lower amplitude, the decoupler is open and fluid passes freely through it, so it will likely not use the inertia track as a passage. It should be mentioned that bulge stiffness of the lower chamber is very high, making the static stiffness of the hydraulic mount almost equal to that of the top elastomeric section. When the frequency increases, the fluid traveling

from the inertia track causes higher damping and results in an increase in the dynamic stiffness until it reaches maximum value, at which point, fluid uses the decoupler to flow between two chambers [15]. Moreover, the static stiffness of the mount is almost the same as the stiffness of rubber located on top of the mount. Modelling of the hydraulic mount is necessary for studying the dynamic stiffness of the mount system. Various researchers modeled the engine mount from one degree of freedom systems to multi-degree linear and nonlinear systems. Royston and Singh [4] discussed the nonlinear properties of passive hydraulic engine mounts in detail. Kim et al. [16] studied passive and adaptive engine mounts with emphasis on their nonlinear characteristics. Golnaraghi et al. [1] developed and analysed the nonlinear model of engine mounts with emphasis on flow resistance of fluid passing through the decoupler. They also analyzed the dynamic characteristics of a hydraulic engine mount with a lumped model based on finite element analysis [2]. Geisberger [17] developed the passive engine mount and derived the time domain equations of a passive mount and identified all parameters of the mount such as linear and nonlinear resistance of the inertia track; in addition he designed a bell added to the mount to obtain better noise isolation. Singh et al. [19] analysed hydraulic engine mount linearly with an emphasis on decoupler characteristics. Wang et al. [20] obtained the graphical modelling method integrated with parameter identification of hydraulically damped rubber mounts by applying the finite element method. With an emphasis on resistance of the inertia track, Shangguan et al. [23], modeled the hydraulic engine mount. They used glycol as a fluid and the least square estimation as a method; they also used the nonlinear finite element method and computational fluid dynamics to study the parameter of the lumped model of a mount [24], and compared the results with experimental data [25]. Wang et al. [49] used ABAQUS software to study the dynamic characteristic of hydraulic damped mounts; as well, they studied [26] the damped mount and analyzed the hydrostatic fluid-structure characteristic of it with emphasis on fluid transfers between chambers. Nakhaei et al. [2] modeled the nonlinear mathematical equations of the decoupler and validated the results with experimental data by using the multiple scale perturbation method. He et al. [27] proposed a nonlinear time domain model for a free decoupler mount to predict both decoupler and inertia track resonances at higher frequencies. Studying the passive engine mount guides us to the point where a typical passive mount has two chambers

with inertia track and decoupler as passages for fluid; it works as a piston to push the fluid to the lower chamber, and also should be sealed perfectly to provide the vacuum inside and pull the liquid back to the upper chamber. Considering the characteristics of those various mounts, it can be concluded that the passive hydraulic engine mount can produce lower dynamic stiffness for vibrations at high frequencies and high damping for shock excitation control; due to its amplitude-and frequency-dependent properties. However, because of the significant nonlinearity of the decoupler, its use is not practical for superimposed impacts. To solve the problem, semi-active and active hydraulic engine mounts are introduced [7].

1.3. Semi-active mount

Semi-active hydraulic engine mounts are created to improve the dynamic performance of conventional hydraulic mounts. Elastic stiffness and damping parameters can be controlled and, as a result, the dynamic response of a mount can be adjusted based on the desired performance. Shoureshi et al. [28] introduced a typical example of a semi-active hydraulic engine mount that contained an external bleed to adjust the spring and damping parameters. In this mechanism, they controlled the system resonance frequency by changing the pressure of fluid injection and by restricting the orifice. Passive engine mount with controllable parameters and mechanism is defined as a semi-active engine mount system. The benefit of these kinds of mounts is that, if the controllable parameters stop working properly, they can still perform as a passive hydraulic engine mount, thereby giving higher reliability than the conventional model. Two kinds of smart material are used by manufacturers in semi-active mounts: Electro-rheological (ER) [29] and Magneto-rheological (MR) [30] fluids. These materials have similar characteristics due to their resistance to flow and their energy dissipation. In some cases, an on-off solenoid valve is added to change the passive mount to a semi-active mount [31]. Winslow [55] developed ER fluids by blending semi-conducting particles and a dielectric carrier liquid. Choi et al. [29] studied the ER engine mount in terms of its feedback control characteristic of shear mode. The noise absorption capability of their proposed model due to random and sinusoidal

excitation has been observed. By using an electro-viscometer, they could determine experimentally the value of the field-dependent yield shear stress of ER fluid, and then implemented the stress into the equation of motion of engine mount. Because of the high working voltage consumption of ER, industries often hesitate to use it. MR fluids are a mixture of magnetically polarisable materials located in a low viscous fluid media [8]. Rabinow discovered that the viscosity of these materials can be adjusted by changing the external magnetic field [33]. The yield strength of MR fluid is 50-100 kPa [32]; and if we remove the magnetic field, MR fluid behaves like Newtonian fluid. Peel et al. [34] were the first to illustrate the capability of MR fluid in noise isolation. Mathematical and mechanical models of MR fluid were derived by Jolly et al. [35] and Davis [36] after industries started to use MR fluid in various applications in the 1980s. William et al. [37] were the first to create a semi-active engine mount; they simulated it mathematically along with experimental results they obtained with their test setup.

In recent models, researchers have inserted a microchip to control vibration isolation that measures the vibration and produces feedback. It also controls the electric current that creates a magnetic field to the hydraulic mount. As a result, when a hydraulic mount starts to vibrate, it pushes MR fluid through the inertia track from the upper chamber to the lower, and vice versa, while the flow of fluid can be adjusted by the magnetic field that induced by microchip [8]. By changing the length of inertia track and effective decoupler area, Foumani et al. [31] used a solenoid valve to tune the mount at low frequency excitation of road condition and high frequency of engine disturbances. They have indicated improvement in performance of the passive mount using their switch. Mansour et al. [30] used the passive engine mount as a base and put an auxiliary MR fluid chamber inside the pumping chamber to function as a pressure regulator. By applying electrical current to the magnetic field, they were able to switch the properties of the mount from passive to semi-active, drawing on desirable characteristics. MR semi-active systems demonstrate low energy consumption, low cost, and very effective isolation characteristics. Semi-active hydraulic engine mounts are used mainly to absorb the noises at lower frequency of excitation; to solve the problem at higher frequencies; active engine mounts have been developed.

1.4. Active mount

An active hydraulic engine mount is a component that isolates engine- and road-induced vibrations; it contains one or more actuators to create dynamic force to restrict the transmission of the system disturbance force. Moreover, energy is conducted continuously inside the engine mount to adjust its dynamic performance and meet target optimization. This kind of mount is used in various industrial engines such as marine, aircraft, and helicopter [8]. An active engine mount is a passive engine with an actuator, a structural vibration sensor, with an added electronic controller. The system works as a closed loop; an actuator provides a reasonable force while a vibration sensor (could be force sensor) sends a controlled signal to the controller; the controller then adjusts the force induced by the actuator to minimize the measured sensor signal, resulting in deduction of the disturbances [7]. As with a semi-active mount, if the actuator or other electrical components fails, the passive part can still perform vibration isolation. Various controlling methods are available for obtaining optimal parameter values in an active isolator; for example, Tuer et al. [56] developed the concept introduced by Golnaraghi [38] about a nonlinear absorber to model the active system. Different types of actuators are being used in active engine mounts; for example, Ushijima et al. [39] studied piezoelectric actuators for these mounts. The reason they investigated these actuators was their fast response; but the problem was limitation of displacement, which makes them not very practical, so they introduced the amplitude magnifying mechanism to solve the problem. Another actuator for use in active mounts is proposed by Fursdon et al. [40], using an electro-magnetic actuator and self-tuning noise cancellation algorithm. They also showed that by adding a voice coil actuator to a passive engine mount and moving it, they could adjust the pressure in the upper chamber of the engine mount, resulting in good isolation in a range of 25-200 Hz. Arzanpour and Golnaraghi [41] offered a novel solution for variable displacement engines. They used a magnetic actuator to produce mechanical pulse, and, by using linearization technique, they were able to simplify the equations. Mansour et al. [57] designed a solenoid valve-based active mount; they replaced the decoupler with a solenoid actuator to control the dynamic characteristics of the mount.

The static stiffness of an active mount is similar to that in the passive one, while the dynamic stiffness is quite different. An active mount can produce high damping and stiffness at lower frequencies, and low damping and stiffness at higher frequencies, providing excellent isolation and allowing the manufacturer to investigate building the cars with lighter bodies. Although these mounts show great performance, their cost and weight still pose a challenge to manufacturers.

1.5. Summary

As discussed, there are three types of engine mounts for use in the automobile industry: passive, semi-active, and active. Car companies in the past, used rubber mounts due to their cheap price and low maintenance fees. Passive engine mounts are no longer as simple as rubber mounts but are still much more economical than the other two models. The advantage of the passive engine mount is its simplicity, making it independent of electrical and control components.

Semi-active engine mounts have a different structure and, along with active engine mounts, improve the functionality of passive engine mounts to absorb vibration and provide the proper damping and stiffness characteristics. In the semi-active engine mount, use of Electro-Rheological and Magneto-Rheological fluids, which are smart materials, enables the manufacturers to build the mount with adjustable resistance, which can be controlled to have the desired performance in any kind of situation [8]. An active engine mount is more complicated and more expensive due to the transducer located inside the mount to create the force needed to modify and control the dynamic performance of the mount and provide a smooth ride for occupants. There are various kinds of transducers for use inside engine mounts, such as piezoelectric actuators, servo-hydraulic actuators, and electromagnetic inertia-mass actuators, depending on their capability and performance. Although semi-active and active hydraulic engine mounts show very good performance at various ranges of frequency, not many car companies rely on them, given their cost and maintenance fees along with their complications. The passive hydraulic engine mount is still the first choice in the car industry because of its simplicity and inexpensive models. Passive hydraulic mounts are

the focus in this thesis. Figure (1-1) shows commercial passive hydraulic engines mount; Figure (1-2) depicts its main rubber, upper and lower chamber, decoupler, and inertia track. In the coming sections, a passive engine mount will be discussed in detail.

Figure 1-1: Hydraulic passive engine mount

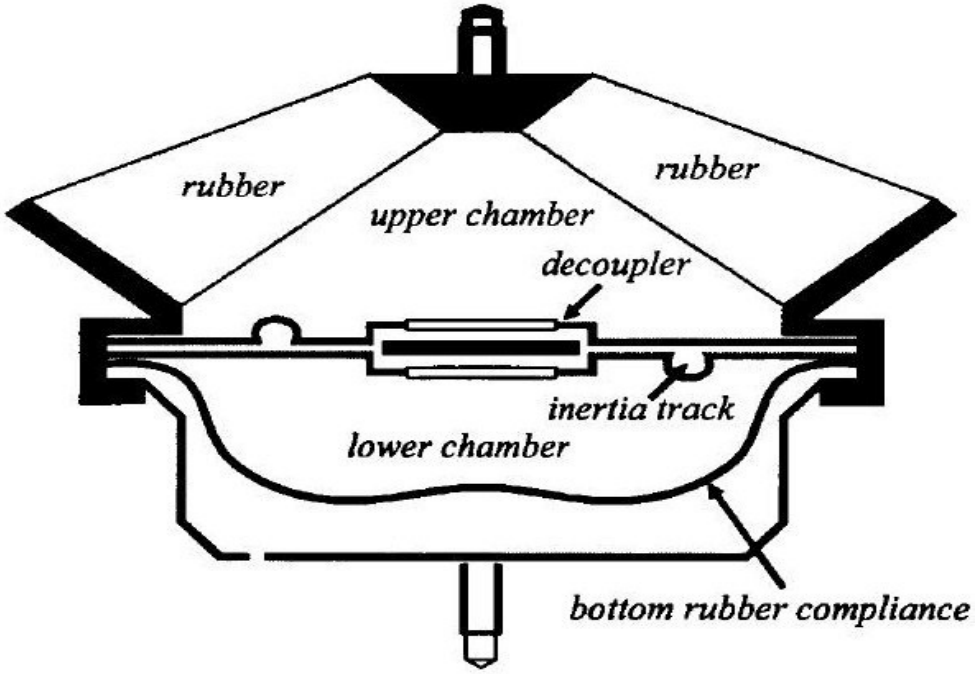

Figure 1-2: Schematic views of hydraulic passive engine mount [1]

1.6. Objectives and thesis outline

In chapter one, the engine mount has been discussed in detail. All kinds of mounts are studied and reviewed with their advantages and disadvantages. It has been showed that the main model to investigate in this thesis is passive hydraulic engine mount and the reasons for choosing this model of mount have been developed. Chapter 2 dedicated to passive hydraulic engine mount with its components. The mechanism and characteristics of a passive engine mount have been discussed. As a background, harmonic excitation of a damped system is studied. Also, analytical modelling of engine mount and its linear equations with the help of its schematic are investigated in detail. Hydraulic engine mount prediction program, HEMPP, is introduced in this chapter, along with problem definition. It is shown that there are discrepancies between the experimental results of frequency response of dynamic stiffness of mount, and simulation data predicted by HEMPP.

Chapter 3 provided a preliminary discussion of the effect of parameters and geometry on the pressure gradient inside pipe. In this chapter, the first experimental setup has been introduced. The pulsatile and reciprocating flow is passed through the regular pipe and the influence of dimensional parameters of pipe on the pressure gradient of fluid has been studied. The effects of roughness, cross sectional area and curvature of pipe have been evaluated. Studying the mechanics of fluid and modelling the pressure gradient equations of pulsatile and reciprocating flow are done in chapter 4. Also the equation of resistance of inertia track is derived in this chapter.

The second test apparatus is introduced in chapter 5 to verify and validate the derived equations of chapter 4. The influence of using different material and also, increasing the resistance on frequency response of dynamic stiffness have been simulated via HEMPP. Moreover, new model of resistance is implemented in HEMPP and final results have been achieved.

Chapter 6 concluded the thesis. The key findings are highlighted and recommendations for future work in this area are discussed.

2. Passive hydraulic engine mount

As discussed in the last chapter, the rubber engine mount could not satisfy dual functionality of high damping and stiffness at lower frequencies and soft at higher frequencies. Also semi-active and active mounts are not economically sufficient for use in all kinds of vehicles. In this chapter, the passive hydraulic engine mount is investigated; its characteristics and performance along with its analytical modelling are studied.

2.1. Desired engine mount characteristics

An engine mount is a vehicle component widely used to attach the engine bracket to the chassis and isolate the power train from road excitation in the vertical direction and torque excitations from the engine around crankshaft. One advantage of the hydraulic engine mount is to provide high damping at certain frequencies. The main factors in designing the hydraulic engine mount (HEM) are: the influence of characteristics of the HEM's rubber spring, the fluid viscosity and density and the geometry of inertia track and decoupler along with the ratio of the maximum dynamic stiffness to the stiffness of the HEM [7].

All these factors must be estimated with the effective models and methods. The engine is connected to the car's chassis by several mounts, which are important for smooth operation of the vehicle. With today's developments in technology, engine mounts come in different sizes and types. In this chapter, we explore the mechanism of the passive engine mount and its components along with its mathematical modelling.

2.2. Mechanism of passive engine mount

A passive hydraulic engine mount contains upper and lower chamber, inertia track, decoupler, and main rubber on top which has same role as in conventional mounts. The fluid within the mount is a mixture of ethylene glycol and water. The decoupler and inertia track are passages for fluid to pass through from the upper chamber to the lower, and come back to the upper chamber from the lower. Compliance of the lower chamber is much greater than in the upper, which expands more than the other one when liquid is pushed to fill the lower chamber. At high frequencies and lower amplitudes, the decoupler is open and all the fluid passes through it between two chambers; at low frequencies and high amplitudes the decoupler is closed and the inertia track plays the main role of circulating the liquid, thereby dissipating energy in the inertia track. This is exactly what manufacturers require; at low frequencies we need high stiffness and high damping and at high frequencies we need low stiffness and low damping, and with this attitude of mount we achieve that goal [22]. The typical hydraulic engine mount is shown in Figure (2-1); Figure (2-2) depicts a schematic of the engine mount with inertia track and decoupler. At top the mount is attached to the engine, and at bottom it is connected to the chassis. Other than isolation of noises, the engine mount should be able to support the weight of the engine, so manufacturers are concerned with choosing the right material to support the engine. Huge disturbances would be created if one of the mounts broke. The mount illustrated in Figure (2-1) is the product of Cooper Standard that contains a bell. Geisberger [17] added the bell to the mount which is used to relieve the resonant frequency of the liquid column of the decoupler. It is attached directly to the point of excitation and adds more flexibility to the high frequency results. In the following sections, all the components of the mount will be discussed in more detail.

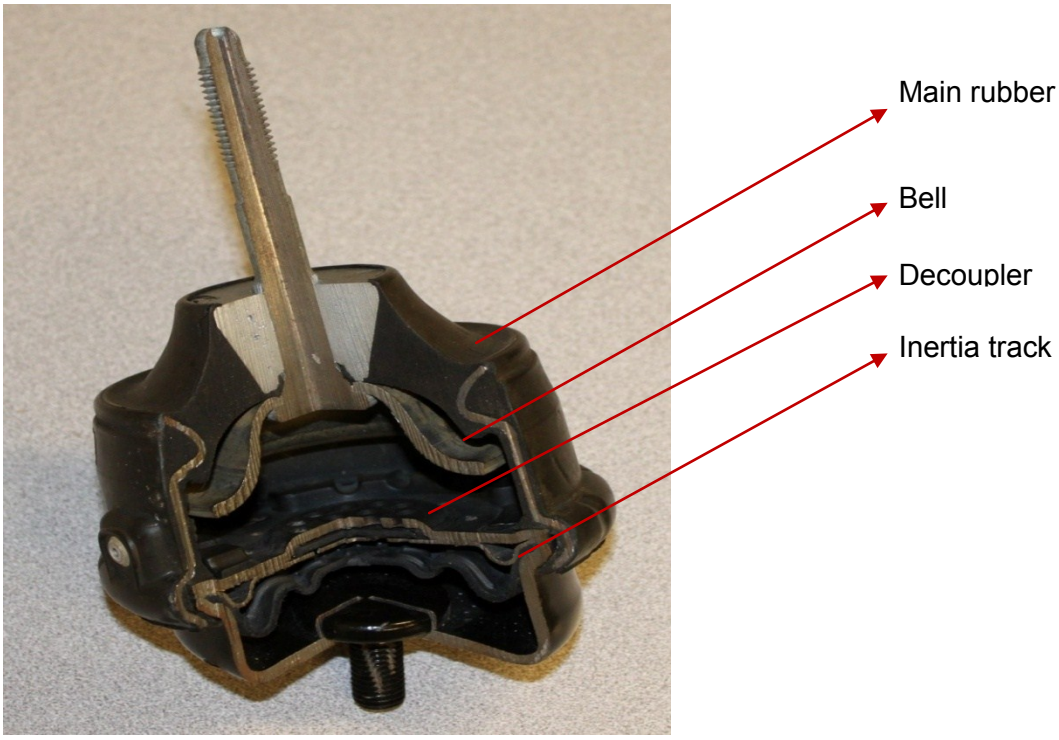

Figure 2-1: Cooper Standard engine mount

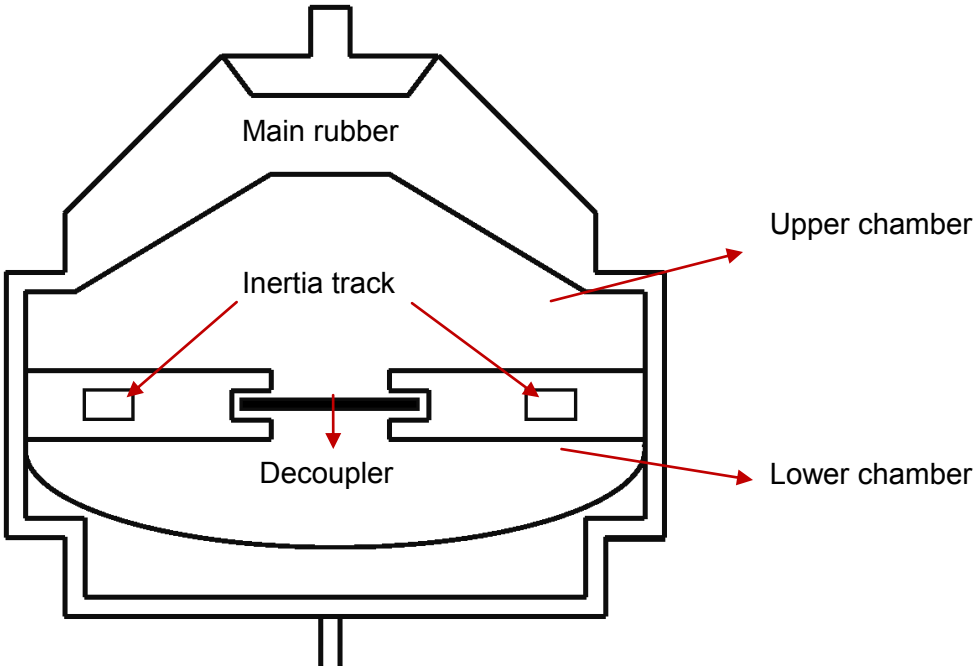

Figure 2-2: Hydraulic engine mount cross section

2.2.1. Upper chamber

The upper chamber is a space between the upper rubber and plate that contains the inertia track and decoupler. Depending on the manufacturers who produce the engine mount, it may contain bell or have the decoupler and inertia track in different sizes. The main rubber has very low compliance that makes it very stiff and at very low frequencies, it has the same role as conventional rubber mounts, and it tolerates the weight of the engine. The rubber is pushed down under the weight of the engine, and vibration of the engine and road condition makes it work as a piston to push the fluid through the decoupler and inertia track to the lower chamber. Because the lower chamber is made of low-stiffness rubber and cannot push the fluid back to the upper chamber, the fluid comes back to the upper chamber because the vacuum develops in the upper part of the mount. The length and width of the rubber on top of the mount change depending on the amplitude and frequency of excitation. In terms of simulation the dynamic stiffness of the mount, modeling the parameters of the rubber such as compliance (C_1), which is better defined as bulging compliance, is difficult and should be done very precisely because of its nonlinear characteristic. This factor depends on some parameters such as frequency of vibration, preload, and volume of fluid inside the upper chamber [17]. Moreover, the fact that upper rubber works as a piston to push the fluid through the gates to the lower chamber, makes the calculation of effective piston area (A_p), important. Geisberger [17] calculated the effective piston area for dry mount and found that this parameter is a function of preload, which is weight of the engine.

2.2.2. Lower chamber

The lower chamber is made of rubber with high compliance, which provides low stiffness. As a result, it expands easily when the fluid is pushed from the upper chamber through the decoupler and inertia track to the lower cage. With its high compliance, the damping characteristics of the lower chamber are much more valuable than its stiffness. Bulging compliance of the lower chamber C_2, has a direct relation to the preload, which

is weight of engine in our case [17]. In building the mount, however, employing the right rubber with the precisely chosen thickness is an important factor. Although the rubber in the lower chamber should have low stiffness and should expand well, it has to have good resistivity. Otherwise it will fracture and leak, damaging the mount and causing disturbances for the occupants.

2.2.3. Decoupler

One of the connections between the upper and the lower chamber for passing the fluid is the decoupler. A decoupler, as depicted in Figure (1-2), is a gate-like cylinder with a few orifices at the top and bottom, and a rubber that moves up and down inside this cylinder shape gate. The mechanism of movement of this rubber depends on the amplitude of excitation. At higher frequencies and lower amplitudes, for example at amplitude of0.1 mm and frequency in the range of 50-250 Hz, the gate is open and the rubber moves freely inside [38]. Furthermore, the fluid moves between two chambers easily, and the inertia track is out of mechanism due to its narrow diameter. On the other hand, when excitation is occurring at lower frequency and higher amplitude, the rubber contacts the orifices and closes the gate, and makes the inertia track the only path for fluid to move between the two chambers. Golnaraghi et al. [1] studied the nonlinear characteristics of a decoupler, along with Singh et al. [19] who worked on the nonlinear characteristics of decoupler, due to the free travel gap for rubber inside the decoupler and diaphragm area. In the Cooper Standard products we are working with, the decoupler has 28 holes of 3 mm diameter, 14 holes on each side. Another consideration that has been investigated by Geisberger [17] is the leakage of the decoupler when its rubber sits on the bottom of the cage. It adds a leakage term to nonlinear equations of the mount. To the matter of fact that we studied the mount at lower frequencies to analyze the attitude of inertia track, as will discussed in the test setup, the decoupler cage has been closed firmly to avoid any leakage and make the inertia track the only passage for fluid from the upper chamber to the lower, and from lower chamber to the upper.

2.2.4. Inertia track

The inertia track is a pipe of small diameter that connects the lower chamber to the upper and fluid passes through it if the decoupler is closed. Its cross section and diameter can be different in each kind of engine mount. Some of the engine mounts have more than one inertia track, based on the dynamic stiffness requirements. Zhang et al. [42] studied the resistance of the inertia track of an engine mount with one, two, and three inertia tracks. In the case of a closed decoupler, the inertia track plays a major role in energy dissipation inside the mount and provides the high damping needed at low frequency to isolate the cabin from noises and vibrations. The inertia track studied in this thesis has a diameter of 5.4 mm and the cross section is semicircular. Many researchers assume the inertia of the fluid inside the inertia track I_i and resistance of fluid R_i are constant. Kim and Singh [19] have considered that the inertia of the fluid in laminar flow inside inertia track increases by frequency. Because the Reynolds number keeps changing due to the sinusoidal excitation of fluid, in this thesis the resistance cannot be assumed to be constant, based on the experimental results and simulations.

2.3. Harmonic excitation of damped system

Before investigating mathematical modelling of the engine mount, we decided to study the harmonic excitation of a damped system, to gain a better understanding of the desired characteristic of engine mounts.

Considering the engine as a mass and the engine mount as a component containing spring and damper, as depicted in Figure (2-3), the mechanical equations of harmonic base excitation are explained [22]. Assuming sinusoidal excitation of the base and summing the relevant forces on the mass m, the sum of gravitational force and two forces acting on mass from damper and spring modeled in Figure(2-3), the equation of motion yields,

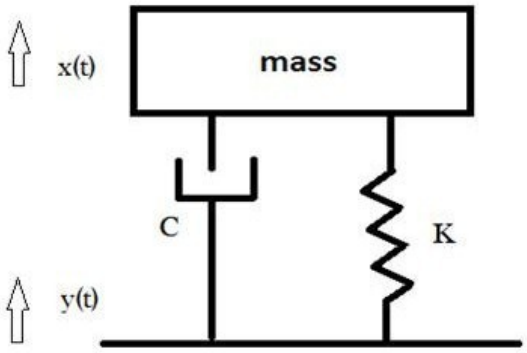

Figure 2-3: Lumped model of mass, spring and damper system

$$m\ddot{x} + c(\dot{x} - \dot{y}) + k(x - y) = 0 \qquad 2\text{-}1$$

with sinusoidal excitation of base:

$$y(t) = y_b sin\omega_b t \qquad 2\text{-}2$$

where y_b represents the amplitude and ω_b denotes the frequency of base oscillation. By substituting $y(t)$ from equation (2-2) into the equation of motion given in (2-1), the following equation is achieved:

$$m\ddot{x} + c\dot{x} + kx = c\omega_b y_b cos\omega_b t + k y_b sin\omega_b t \qquad 2\text{-}3$$

If we use the definition of natural frequency and damping ratio [22], then calculating the particular solution of equation (2-3) and dividing by the mass yields,

$$\omega_n = \sqrt{\frac{k}{m}} \qquad 2\text{-}4$$

$$\zeta = \frac{c}{2m\omega_n} \quad \text{2-5}$$

$$\ddot{x} + 2\zeta\omega_n\dot{x} + \omega_n^2 x = 2\zeta\omega_n\omega_b y_b cos\omega_b t + \omega_n^2 y_b sin\omega_b t \quad \text{2-6}$$

where ζ is damping ratio, c is damping coefficient and ω_n is natural frequency.

Equation 2-6 be simplified as

$$\ddot{x} + 2\zeta\omega_n\dot{x} + \omega_n^2 x = y_b\sqrt{\omega_n^4 + (2\zeta\omega_n\omega_b)^2}\, cos(\omega_b - \theta) \quad \text{2-7}$$

Considering $f_0 = 2\zeta\omega_n\omega_b$ and solving the equation for particular and harmonic solution we obtain

$$x_p = \frac{f_0}{\sqrt{(\omega_n^2 - {\omega_b}^2) + (2\zeta\omega_n\omega_b)^2}} cos(\omega_b t - \theta - \theta_1) \quad \text{2-8}$$

and

$$x_p = \frac{y_b\sqrt{\omega_n^4 + (2\zeta\omega_n\omega_b)^2}}{\sqrt{(\omega_n^2 - {\omega_b}^2) + (2\zeta\omega_n\omega_b)^2}} cos(\omega_b t - \theta - \theta_1) \quad \text{2-9}$$

for θ and θ_1, By definition

$$\theta = tg^{-1}\frac{\omega_n}{2\zeta\omega_b} \quad \text{2-10}$$

$$\theta_1 = tg^{-1}\frac{2\zeta\omega_n\omega_b}{\omega_n^2 - {\omega_b}^2} \qquad 2\text{-}11$$

Therefore, knowing that time goes to infinity and defining r, frequency ratio, we get

$$\frac{x}{y_b} = \frac{\sqrt{1 + (2\zeta r)^2}}{\sqrt{(1 - r^2)^2 + (2\zeta r)^2}} \qquad 2\text{-}12$$

$$r = \frac{\omega_b}{\omega_n} \qquad 2\text{-}13$$

which expresses the ratio of the maximum response magnitude to the input displacement magnitude which is used to define the transmission of motion from the base to the mass as a function of frequency ratio $\frac{\omega_b}{\omega_n}$.

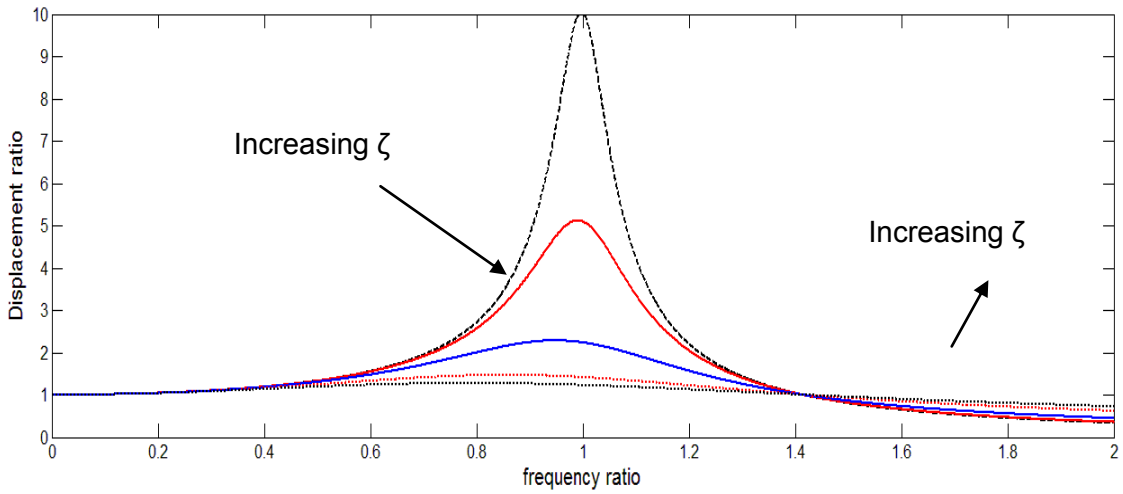

Figure 2-4: Displacement transmissibility as a function of the frequency ratio [22]

The graph in Figure (2-4) makes it obvious that for $\mathrm{r} < \sqrt{2}$, the transmissibility ratio is greater than 1, which shows that motion of the mass is an amplification of motion of the base, and a different value of damping ratio ζ determines the level of amplification. It is also seen that for $\mathrm{r} > \sqrt{2}$, the transmissibility ratio is less than 1, and motion of the base is larger than motion of the mass. Knowing that the best situation is to have the transmissibility ratio between 0 and 1, we need to have an interchangeable attitude based on frequency and amplitude of the system. This graph directs us to the conclusion that at low frequency and high amplitude, we need higher damping ratio *ζ* and stiffness *K* and damping coefficient C, but at high frequency and low amplitude we need lower *ζ* and *K* and *C*. To achieve these responses we are using a passive engine mount that has different attitude based on various frequencies.

As discussed, the ideal engine mount should minimize the transmissibility ratio of the engine to the chassis. Therefore, having low damping for $r > \sqrt{2}$ and increasing the frequency ratio to move to the right of Figure (2-4) are desirable. To achieve these, we must decrease the stiffness of the engine mount along with damping coefficient. Considering $r < \sqrt{2}$, at the lower frequency region in Figure (2-4) the mount must provide higher damping ratio and stiffness to reduce the transmissibility. The design of

the hydraulic engine mount is a time-consuming, expensive process needing many trial and error attempts, so to save time and energy, good modeling of passive engine mounts is required.

2.4. Linear model of hydraulic engine mount

A linear model of the hydraulic engine mount with emphasis on the inertia track as the main passage of fluid inside the mount has been investigated. Figure (2-5) illustrates a lumped model of our passive engine mount, with the decoupler and inertia track as paths for fluid from the upper chamber to the lower, and vice-versa. As depicted in Figure (2-5), K_r is the stiffness of the main rubber while, b_r is the damping coefficient of the rubber on top of the mount. Assuming the chambers of engine mount are a cylinder and movement of the upper rubber is a piston, A_p is the effective piston area. In addition, Q_d and Q_i are flow rate passing through the decoupler and inertia track, and M is the mass of engine, X and y being the motion of engine and hydraulic mount, which is attached to the chassis. Finally, C_1 and C_2 are compliances of upper and lower cage, while $P_1$and P_2 demonstrate the pressure of upper and lower chamber. Now we can study momentum equations for an engine mount.

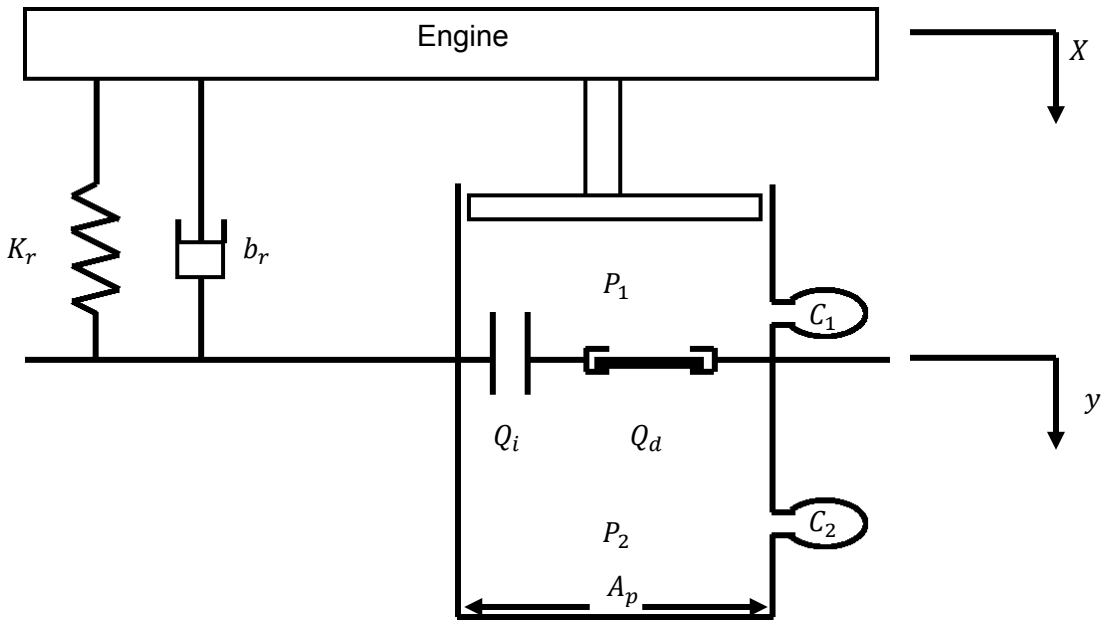

Figure 2-5: Lumped model of hydraulic mount [17]

$$C_1\dot{P}_1 + Q_i + Q_d = A_p\dot{X} \qquad 2\text{-}14$$

$$C_2\dot{P}_2 = Q_i + Q_d \qquad 2\text{-}15$$

Because the focus of this project is response of the engine mount at lower frequencies, and knowing that the inertia track is the main passage for fluid at this frequency range, the decoupler is assumed to be closed in deriving the equations.

2.5. Linear equations for fixed decoupler

Assuming we use a fixed decoupler, we can write equation (2-14) as

$$C_1\dot{P}_1 + Q_i = A_p\dot{X} \qquad 2\text{-}16$$

$$C_2\dot{P}_2 = Q_i \quad \text{2-17}$$

$$Q_i = A_i\dot{x}_i \quad \text{2-18}$$

where A_i is the cross sectional area of inertia track and $\dot{x}_i$ is the speed of the flow that is passing through inertia track. We can also define C_1 and C_2, upper and lower compliances, as [43]

$$\frac{1}{C_1} = \frac{K_1}{A_p^2} \quad \text{2-19}$$

$$\frac{1}{C_2} = \frac{K_2}{A_p^2} \quad \text{2-20}$$

Where $K_1$and K_2 are stiffness of upper and lower chambers. Considering F_1 and F_2as hydraulic forces induced in the entrance and exit of the inertia track, the following equation can be derived

$$F_1 - F_2 = M_i\ddot{x}_i + b_i\dot{x}_i \quad \text{2-21}$$

Where M_i is finite mass that passes through the inertia track and b_i is the viscous friction in the pipe. Dividing both sides of the equation by the cross sectional area of inertia track, enables us to show the pressure of both sides of the inertia track

$$\frac{F_1}{A_i} - \frac{F_2}{A_i} = \frac{M_i}{A_i}\frac{1}{A_i}(A_i\ddot{x}_i) + \frac{b_i}{A_i}\frac{1}{A_i}(A_i\dot{x}_i)$$

yields

$$P_1 - P_2 = \frac{M_i}{A_i^2}\dot{Q}_i + \frac{b_i}{A_i^2}Q_i \qquad 2\text{-}22$$

Now we can define inertia and the resistance of the fluid inside the inertia track as

$$I_i = \frac{M_i}{A_i^2} \qquad 2\text{-}23$$

$$R_i = \frac{b_i}{A_i^2} \qquad 2\text{-}24$$

Finally the difference of pressure in upper chamber and lower chamber is derived from

$$P_1 - P_2 = I_i\dot{Q}_i + R_iQ_i \qquad 2\text{-}25$$

where P_1 and P_2 denote the pressure of lower and upper chamber, I_i is inertia terms of inertia track, R_i is resistance of the inertia track, and $Q_i$and $\dot{Q}_i$ are volumetric fluid flow and its derivative.

Therefore, to obtain the force transmitted to the basis, we have

$$F_T = K_rX_r + b_r\dot{X}_r + A_p(P_1 - P_2) + A_pP_2 \qquad 2\text{-}26$$

Where K_r and b_r are stiffness and damping of the main rubber. To solve the equations for pressure in the upper and lower chambers as well as fluid flow through the inertia track, the Laplace transformation has been applied to equations (2-16), (2-17) and (2-25), yielding

$$P_1(s) - P_2(s) = sI_iQ_i(s) + R_iQ_i(s) \quad \text{2-27}$$

$$C_1sP_1(s) + Q_i(s) = A_psX_es \quad \text{2-28}$$

$$C_2sP_2(s) = Q_i(s) \quad \text{2-29}$$

As a result, we obtain

$$Q_i(s) = \frac{sA_pX_e(s)}{C_1\left(I_iS^2 + R_is + \frac{1}{C_1} + \frac{1}{C_2}\right)} \quad \text{2-30}$$

$$P_1(s) = \frac{A_pX_e(s)(\ I_iS^2C_2 + R_isC_2 + 1)}{C_1\left(I_iS^2 + R_is + \frac{1}{C_1} + \frac{1}{C_2}\right)} \quad \text{2-31}$$

$$P_2(s) = \frac{A_pX_e(s)}{C_1C_2\left(I_iS^2 + R_is + \frac{1}{C_1} + \frac{1}{C_2}\right)} \quad \text{2-32}$$

Finally, to show the dynamic stiffness of the engine mount, as well as implementing equations (2-31) and (2-32) in equation (2-26), we divide both sides of equation (2-26) by the movement of the engine, assuming the chassis is fixed; then

$$K_d(s) = \frac{F_T(s)}{X_e(s)} = K_r + b_rs + \frac{A_p^2}{C_1}\frac{I_iS^2 + R_is + \frac{1}{C_2}}{I_iS^2 + R_is + \frac{1}{C_1} + \frac{1}{C_2}} \quad \text{2-33}$$

where K_r and X_e are stiffness of main rubber and engine displacement, and A_p denotes affected piston area. Equation (2-33) includes the sum of three components; the

first and second parts are related to the stiffness and damping of the rubber and the third part is the participation of hydraulic components.

Now is a suitable time to analyze the inertia track in terms of its resistance by employing experimental setup to gather reliable data. In next chapters, test apparatus and modeling the resistance of inertia track will be discussed. Although this model seems to be close to real situation, there are still some uncertainties. Assuming the decoupler is closed at lower frequencies and inertia track is only passage of fluid is not very accurate due to leakage of fluid in decoupler area. Also nonlinear characteristic of resistance of inertia track make the linear assumption doubtful. Geisberger [17] added the nonlinear term to solve the problem and have got equation below with R_{i1} and R_{i2} as linear and nonlinear resistances, which is still inaccurate and not perfect solution to model the engine mount.

$$P_1 - P_2 = I_i \dot{Q}_i + (R_{i1} + R_{i2}|Q_i|)Q_i \qquad 2\text{-}34$$

2.6. HEMPP

Hydraulic Engine Mount Prediction Program, HEMPP, is a tool to predict the dynamic stiffness for hydraulic engine mounts over a specified range of frequency values. This software combines experimental data and analytical modeling of engine mount to achieve a better prediction of dynamic attitude of the engine mount at a wide range of frequencies. The dynamic stiffness of a mount can be anticipated by simply inputting various dimensional parameters of the mount along with some other test data, saving both time and cost. The HEMPP uses database files as a compliance files obtained from experiments such as pumping area of upper chamber, stiffness and damping of the main rubber. It should be mentioned that the stiffness and damping characteristics of rubber would be achieved by testing a dry mount, while the effective pumping area at different frequencies have been obtained with a mount full of liquid. The HEMPP then adds the geometrical parameters of the decoupler and inertia track (not in a wide range), and by using an analytical method it can predict the dynamic stiffness of

the engine mount. As depicted in Figure (2-6), in the interface of the program, the manufacturer is able to simulate the behaviour of an engine mount by substituting the right data for the geometry of the decoupler and inertia track, and excitation condition such as range of frequency and amplitude of oscillation. Although the HEMPP is not time-consuming and is simple to understand, due to inaccurate modeling of the engine mount the results do not agree well in a specific range of frequencies.

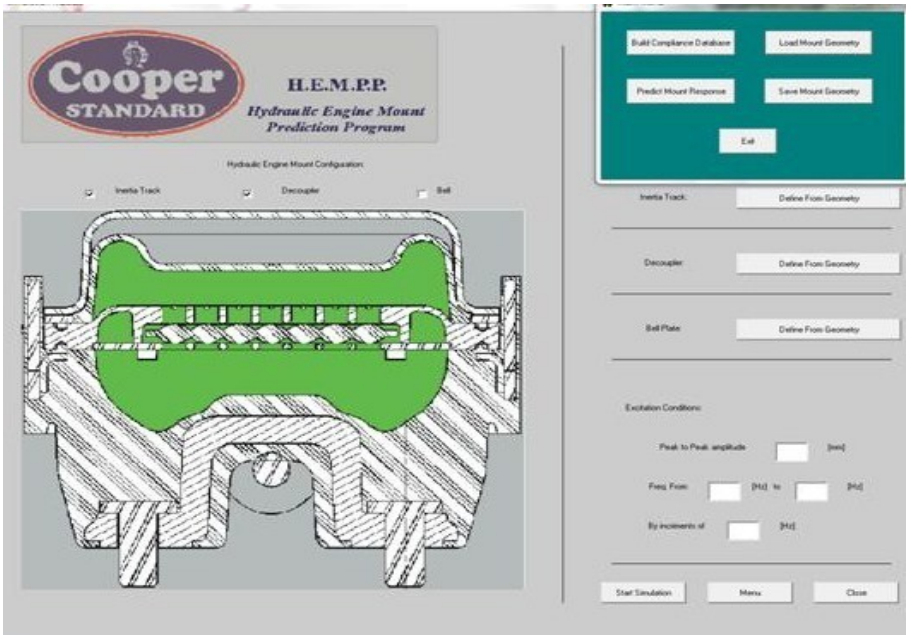

Figure 2-6: Interface of HEMPP

2.7. Problem description

Cooper-Standard Automotive is today one of the leading global automotive suppliers offering solutions in many aspects of industry. Their expertise lies in supply customized products, offering numerous benefits for costumers. An engine mount is an anti-vibration segment that they produce by using a HEMPP. Ultimately, the program is used by company to meet customer requirements without having to use practical trial and error. However, the outputted stiffness curve of the program, HEMPP, fails to generate precise solutions for larger displacement amplitudes, based on comparison

with experimental results. Figures (2-7) and (2-8) illustrate the comparison of simulated results of the HEMPP and experimental results in cases of dynamic stiffness and phase.

Since the prediction begins to fail in the region 10 to 15 Hz, where the inertia track has more dominance on the stiffness output and is the range where the inertia track plays a main role, it has been suggested that the model for resistance of the inertia track could be the cause. For this reason, the goal of this thesis is to precisely identify the resistance of inertia track and to analyze the effect of dimensional divergence on pressure loss under sinusoidal frequency excitation.

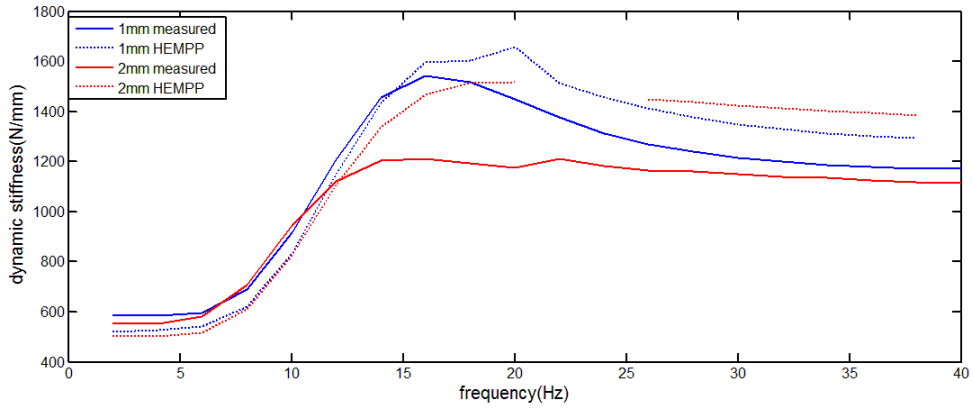

Figure 2-7: Dynamic stiffness outputted by HEMPP and experiments for 1mm and 2mm amplitude of excitation

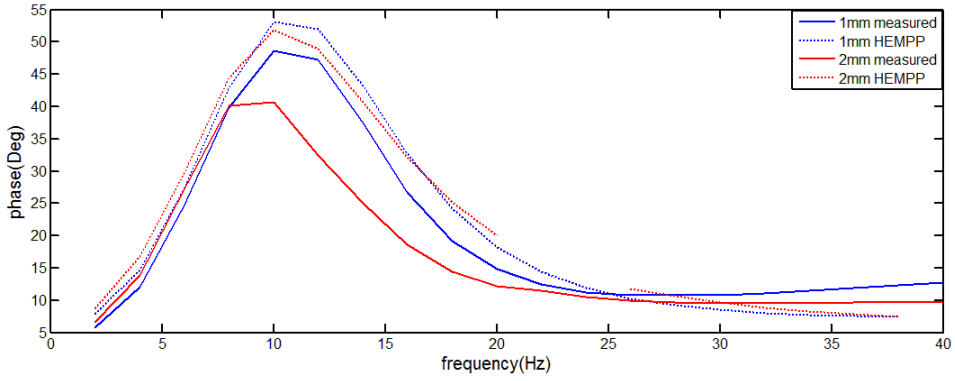

Figure 2-8: Phase outputted by HEMPP and experiments for 1mm and 2mm amplitude of excitation

3. Preliminary Studies on Parameter to Geometry Relation

Before starting the modeling of the resistance of fluid inside the inertia track, we try to get some knowledge of the attitude of pulsatile fluid. This chapter focuses on providing insight into the relationship between dimensions of pipe and its resistance, when fluid inside the pipe is under frequency and sinusoidal excitation. Specifically, the work presented here investigates the effect of roughness, cross sectional area, and curvature of pipe on the frequency response of pressure drop using the experimental procedures described in this chapter.

Using different pipes with different diameters and roughness, and changing the pipe from a straight form to a rotated form in different angles, have been considered. To obtain results from this kind of situation, use of the simple experimental setup discussed in this chapter has been suggested.

3.1. Experimental setup

The experimental setup used to obtain the test data contains the cylinder, piston, and cap that the regular pipe has come out of it. The cylinder is filled with water; this filling should be done precisely to prevent air bubbles from sticking to the walls of the chamber, because bubbles can cause great uncertainties in the results. One pressure sensor model Omega PX481A with ability to sense pressure up to 100psi and producing output in voltage has been located in the end of the cylinder. By putting the sensor there, the pressure of the fluid at the entrance of the pipe is achievable; and because the other end of the pipe is connected to the atmosphere, we can calculate the pressure differences of fluid flowing in the pipe. After the system has been perfectly sealed, we put the whole setup on an electro-magnetic shaker with ability to create a wide range of

frequencies from 5 to 2000 Hz with amplitude of 1” (2.54 cm). This shaker can tolerate 150 kg of mass on top. Then the chassis and holder bar are used to fix the top of the test setup and allow the piston to move up and down inside the cylinder. There is one power field to create the electrical field and one amplifier to induce the power through the shaker for running the test. Also, it is required to have one USB shaker controller to direct and modify the signals to the computer, allowing us to read the data and analyze them. The software used to program the shaker and run it in the desired mode is working through the USB controller. In addition, there is one accelerometer located on top of the shaker to close the electrical loop. The controller has eight input channels as directors of signals those are coming from sensors depends on the condition of the test. In our case that we have two sensors, two of the channels have been used. All the facilities that have been used to run the tests are shown in Figure (3-1). Figure (3-2) shows the test apparatus and its schematic. More information about electro-magnetic shaker and sensors is provided in the next sections.

Power field

Amplifier

USB controller

Shaker and frame

Figure 3-1: Experimental setup and its components

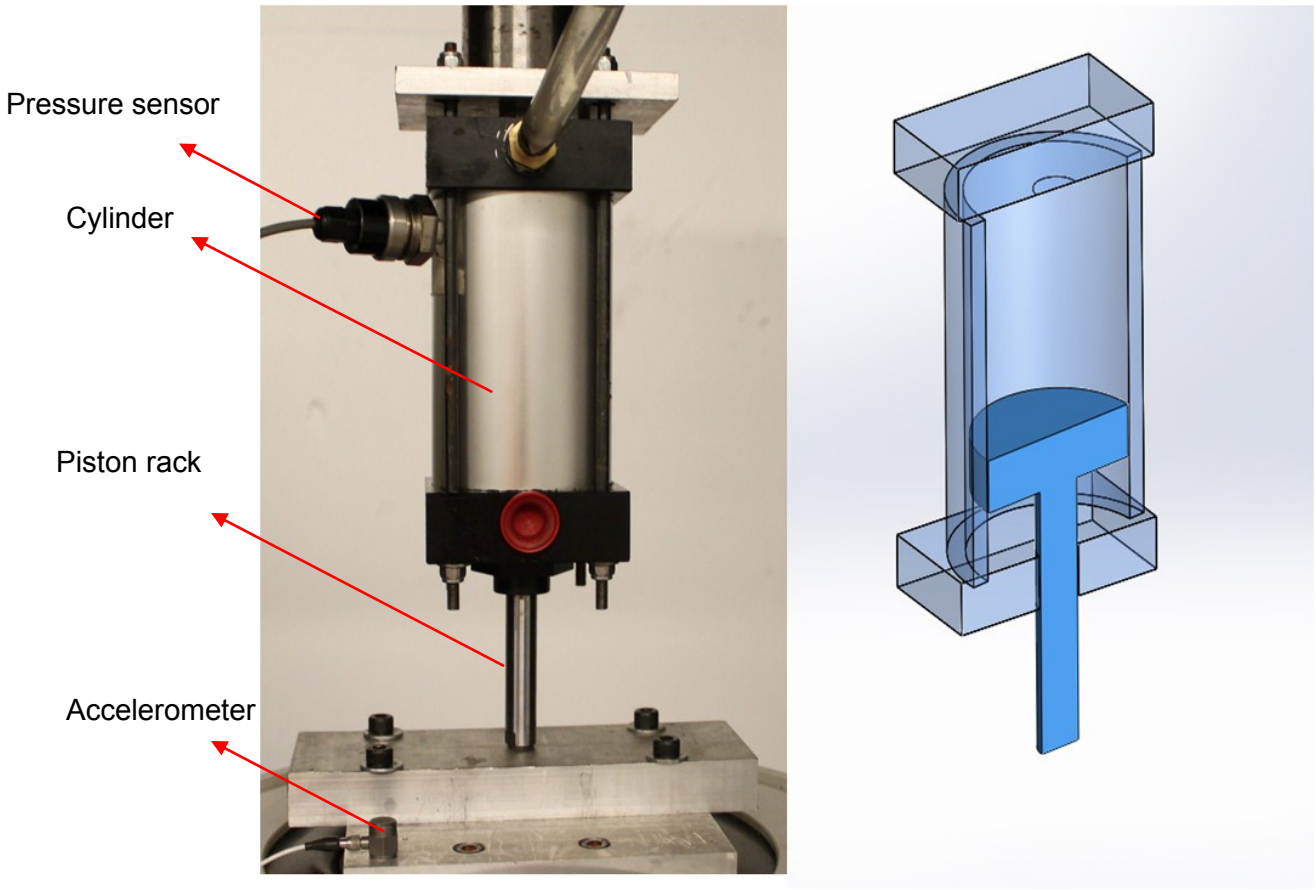

Figure 3-2: Test apparatus and its schematic view

3.1.1. Electro- magnetic shaker

The V721series vibrators are wide frequency band electro-dynamic transducers capable of producing a sine vector force of 4100N (922lbf). These vibrators normally operate in the frequency range 5 to 4000 Hz from a sine wave of random signal input, and are driven by power amplifiers of up to 2.5 KV output. Operation below 5 Hz is possible with a suitable amplifier. They are fitted with built-in air load support with a maximum payload capacity of 100 kg (220lb) with full relative displacement.

The vibrator consists of a magnetic structure that houses and supports the armature and field coils, which are suction air cooled by using a remotely located fan. Degauss coils are fitted to reduce the stray field above the armature table.

The vibrator can be locked in the vertical or horizontal position by means of clamp bolts. On the other hand, it can provide a support about which it can turn in a vertical position. This series of vibrators can be driven by any suitable oscillator/amplifier/field power supply combination, but the LDS PA1000L amplifier is used for this purpose. It also requires a field power supply, the LDS model FPS10L. The typical V721 vibrator is shown in Figure (3-3). Swept-Sine is a common type of vibration test as the name implies, the drive signal to the shaker is a sine wave that changes in a smooth continuous manner over a range of frequencies. The amplitude level of the reference profile can be defined in acceleration, velocity or displacement units. The control system generates an output sine wave to excite the device being tested. A level detector measures the control signal amplitude. The control signal amplitude is then compared with the reference amplitude and the drive signal amplitude is updated.

Figure 3-3: LDS electro-magnetic shaker

3.1.2. Accelerometer

For this test apparatus, the accelerometer model Dytran has been used. This type of accelerometer features Low Impedance Voltage Model (LIVM) operation. The self- generating seismic element, using piezo-ceramic crystals in a planner shear mode, converts acceleration to an analogous electrostatic charge mode signal.

These models are capable of driving long cables with no appreciable effect on sensitivity and frequency response. Simple constant current type power units supply power to operate the integral charges amplifier and separate the signal from the DC bias at the output of the internal amplifier. In our experiments, it is attached to the USB shaker controller which provides the power to run it and get the feedback at the same

time. A coaxial cable has been used to connect the accelerometer to a controller. The other reason to apply this model relates to featuring signal ground isolation on the mounting surface which is at the top of the shaker to avoid annoying ground loops and hermetic sealing for normal operation in moist and dirty environments.

Figure 3-4: Dytran accelerometer

3.1.3. Pressure transducer

A pressure sensor model Omega's PX481A has been installed at the wall of the cylinder. This type of transducer is designed for general industrial requirements and offers excellent performance in a wide range of applications. It is based on proven micro-machined silicon technology, providing high reliability and long-term stability. To avoid damage from high pressure during fast motion, the 100psi range has been chosen. The PX481A is fully digitally compensated for the effects of pressure and temperature change. It is extremely accurate less than 0.3% FS reference accuracy, and less than 1% FS over its compensated temperature range. Wetted parts are made of 316L stainless steel for a wide range of media compatibility, it has voltage output matched to the controller, and it prevents use of the amplifier which may result in more noise in the data obtained.

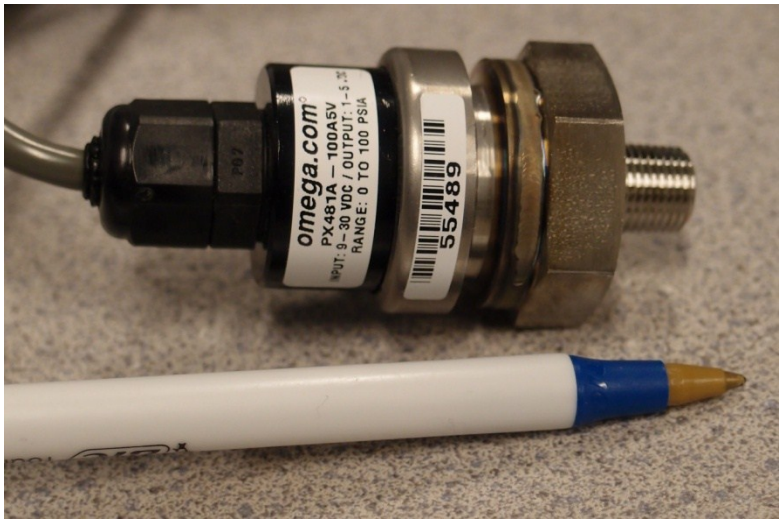

Figure 3-5: Pressure transducer

3.2. Effect of roughness on frequency response of pressure gradient inside pipe

Changing the roughness of the pipe was achieved by locating two different sand papers inside the same 0.5" diameter pipes. As depicted in Figure (3-6), sand papers of 220 grit and course 80 grit were applied inside the pipe. The roughness of 220 grit sand paper is 0.48 μm, and of 80 grit is 1.8 μm. The shaker was programmed to run in sinusoidal motion from 5 to 40 Hz frequency with amplitude of 0.1 mm peak to peak. As illustrated in Figure (3-7), roughness has a great effect on the peak value of the amplitude of frequency response of pressure difference in the fluid flow between two heads of pipe. Although the peak values occur in the same frequency for both situations, the amplitude of the pressure in the smoother pipe is lower than in the coarser one at frequency range 12 to 17 Hz. Based on Bernoulli equation ($\Delta P = f \frac{L}{D} \frac{V^2}{2}$)[44], there are few parameters such as viscosity, dimension and inertia which affect the pressure gradient inside the pipe. At lower frequencies, the interior diameter of the pipe with smoother sand paper is larger than another one, allowing the fluid passes through the pipe with higher speed, causing larger pressure gradient. But at the frequency range 12 to 17 Hz, viscosity shows more effect and pressure gradient in the pipe with coarser

interior is higher than the other one. After this frequency range, the velocity of fluid inside the pipe is larger, inertia dominates the effect of viscosity and pressure gradient inside the smoother pipe becomes larger than pressure gradient inside the pipe with coarser interior. This proves that if we have two pipes of the same size with the same fluid passing through them, the pipe with greater roughness induces more pressure differences between two heads of pipe at specific frequency range.

To study the phase lag of motion, we need to study the Womersley number which is very helpful in understanding the attitude of oscillatory flow. The Womersley number is a dimensionless number that define the collaboration of pulsatile flow frequency with viscous effects. Womersley [45] showed that when the Womersley number is small, flow will be almost in phase with the pressure gradient, but when it is large (greater than 10), flow lags the pressure gradient by about 90 degrees. Womersley number in defined in equation 3-1 with R is radius of the pipe, ω is angular frequency while, μ and ν denote density, dynamic viscosity and kinematic viscosity of the fluid.

$$\alpha = R\left(\frac{\omega}{\nu}\right)^{0.5} = R\left(\frac{\omega\rho}{\mu}\right)^{0.5} \qquad 3\text{-}1$$

Studying the graph in Figure (3-8) of the phase-lag between the pressure of the fluid flow inside the pipe and the acceleration of the fluid leads us to the point where the largest phase lag (180degree) occurs in the same frequency that peak values of pressures take place for both pipes. As depicted in Figure (3-8), at higher frequencies the phases are less than 180 degree and around 140degree, which are reasonable values due to the higher roughness and lower speed of water inside the pipes. Based on work by Womersley [45], it is obvious that increasing the speed of flow caused by the shaker at higher frequency excitation makes the acceleration lag the pressure gradient from zero in 1 Hz frequency up to 180 degree at higher speeds. By looking at the phase graph more closely, it has been observed that the phase of pipe with smoother interior reaches the point of 180 degree phase shift at higher frequency compared with the one that has rougher wall. At lower frequencies, acceleration of the fluid also lags the

pressure gradient in a smoother pipe more than in the rougher pipe. Therefore the roughness in pulsatile reciprocating fluid flow has an undeniable effect.

Figure 3-6: Different sand papers and a pipe

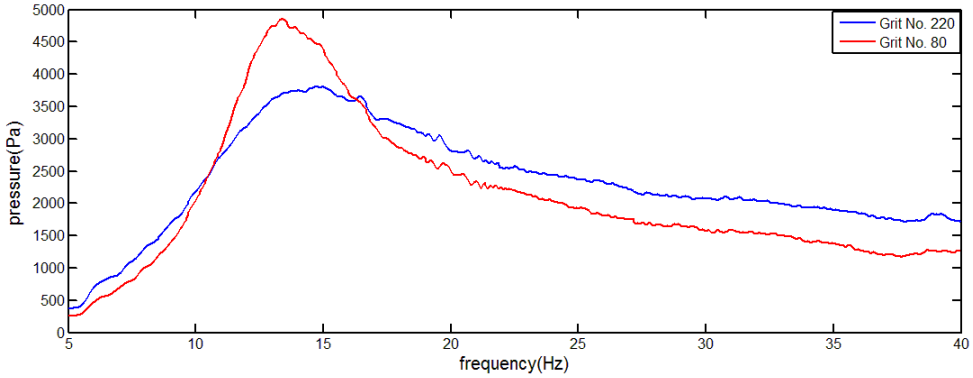

Figure 3-7: Pressure vs. frequency for different pipes roughness

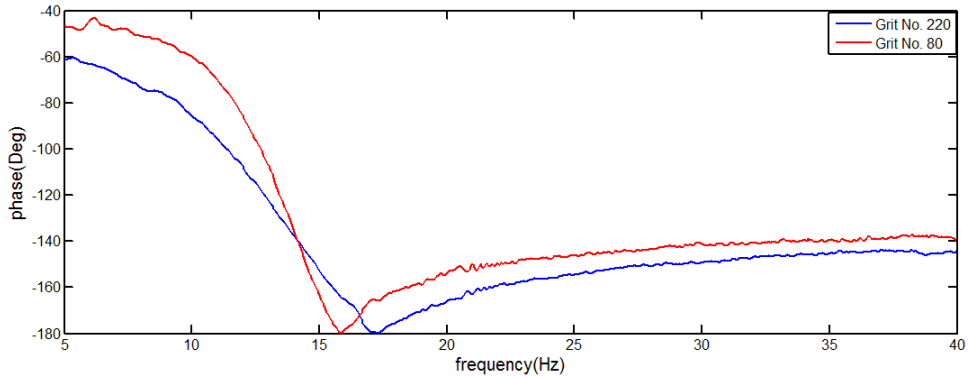

Figure 3-8: Phase lag between pressure and acceleration of flow for different roughness

3.3. Effect of diameter on frequency response of pressure gradient in sinusoidal movement

To observe the effect of change of diameter on frequency response of pressure gradient of fluid flows under the situation of pulsatile reciprocating excitation, three different pipes have been used to the test setup .The Shaker was programmed to run a sinusoidal pattern from 5 to 40 Hz with 0.1 mm peak-to-peak amplitude and a rate of 1 Hz frequency per second, so the total process took 40 seconds. Looking at the results in Figure (3-9), gathered from the pressure sensor located in the same place as in the previous experiment, we reach the conclusion that when the pipe is smaller in diameter, the peak value of pressure gradient occurs at smaller frequency and the value is larger than those with larger cross sectional area. Although all three of them follow the same trend in their frequency response, a smaller cross section creates a higher pressure. As in previous cases, the White's equation can confirm that our experimental results are reasonable; in the pressure differentiation between two heads of pipe, ΔP is related to diameter of pipe, D. It has been proven that $\Delta P \propto \frac{1}{D^4}$ [44]. Studying the loss angles of these three pipes depicted in Figure (3-10), again is showing us that the resonance of frequency response occurs at 180 degree phase lag but depends on the diameter of the pipe; the pipe with smaller cross sectional area reaches the point of the highest phase shift earlier than those with larger cross sectional area. Also, same as previous

experience and considering Womersley number [45], the phase between pressure gradient and acceleration of the fluid starts at 1 and increases to 180 degree, which results in 90 degree loss angle between the pressure gradient and velocity of liquid. So these experimental results prove that the diameter of the pipe has a definite effect on pressure differential, the smaller the pipe, the higher the pressure.

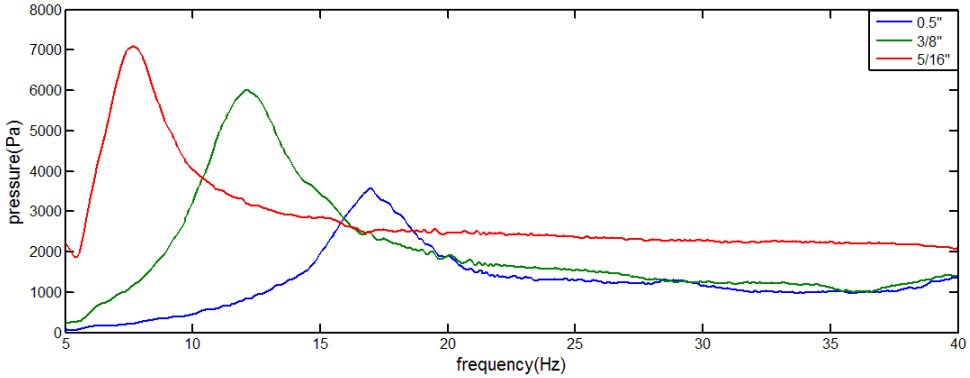

Figure 3-9: Pressure vs. frequency for different diameter

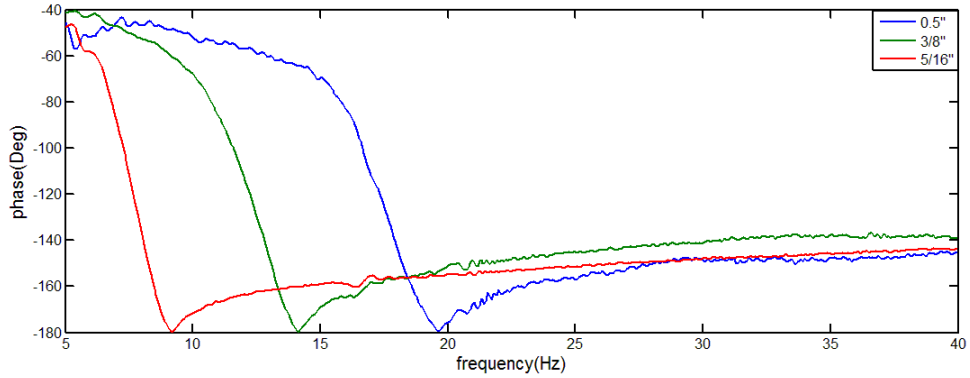

Figure 3-10: Phase of pressure and acceleration

3.4. Effect of curvature on frequency response of pressure gradient in sinusoidal movement

To evaluate the effect of curvature on the frequency response of pressure differentiation of a pipe, when the pulsatile reciprocating fluid flows inside it, the regular

pipe with an inner diameter of 3/8” and accepted flexibility has been used. The reason that the regular transparent pipe was used is the ease of rotating it around the circular cylinder to test different rotational angles. As depicted in Figure (3-11), the 3.25” cylinder made with aluminum has been used as a base, and the pipe was rotated around it, startingat90 degree. Next angle was 180 degree, and rotation continued until the pipe made a circle in increments of90degrees. It has been suggested to use the pipe with smaller diameter because rotating and forming it to the expected shape is simpler than for those with larger cross sectional area.

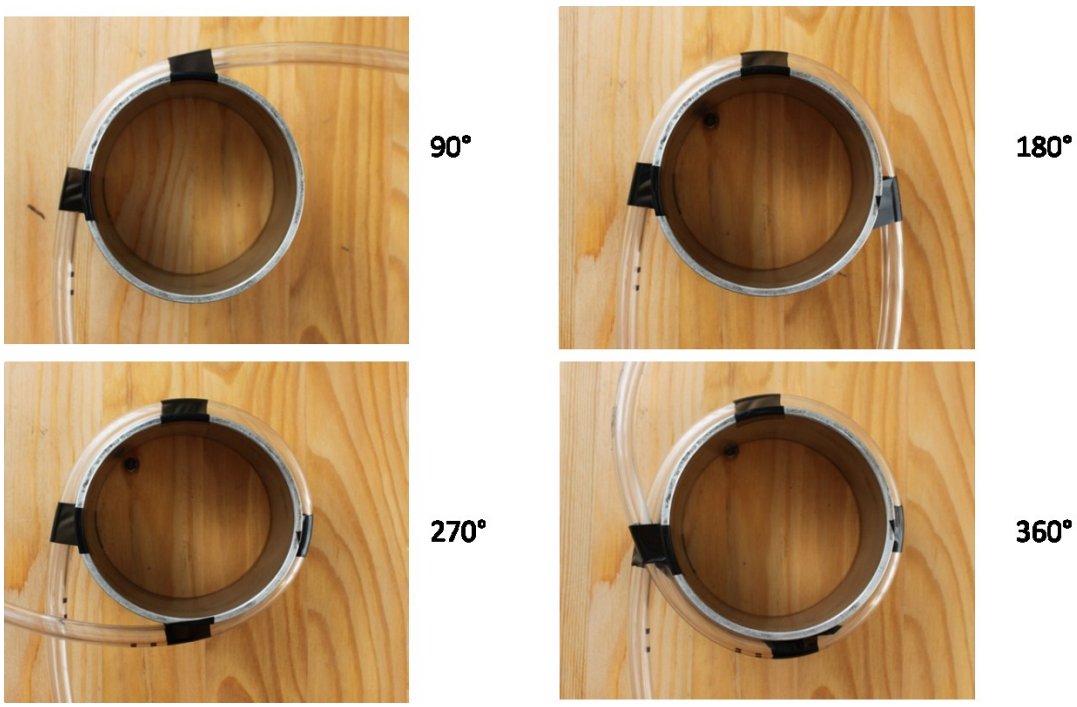

Figure 3-11: Cylinder and pipe rotated around it

To start the test, for each kind of situation and angle, the shaker was programmed to run the sinusoidal motion from 5 to 40 Hz with the rate of 1 Hz per second. Amplitude of excitation was 0.1mm for all of them. The results for frequency response and phase shift are depicted in Figures (3-12) and (3-13). These experimental results lead us to the point where the angular rotation of the pipe does not make a noticeable change in the peak value of the pressure differential of the fluid flows through the pipe, and same for phase; the discrepancy in different angles is negligible. Although entrance loss is a substantial parameter in laminar and turbulent flow [44], in

reciprocating flow in a pipe with small size of cross sectional area and length, it seems to be inconsequential in modelling the fluid flow. Although curvature of the pipe did not have a noticeable effect on the frequency response of the pressure gradient in our study, it has an undisputable influence on the pressure gradient of a pipe when fluctuating fluid flows in bigger pipes with larger cross sectional area and more rounds of circulation. As in previous tests, in this case, the phase between pressure and acceleration of fluid goes up to 180 degree which is reasonable according to Womersley [45].

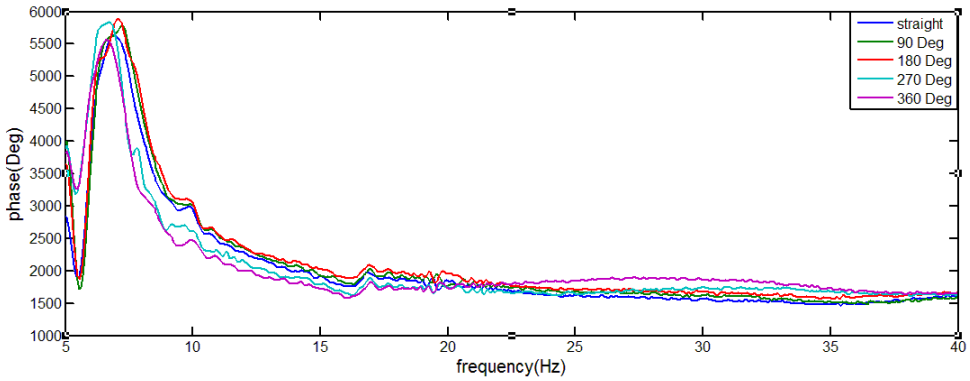

Figure 3-12: Pressure vs. frequency in different rotational angles

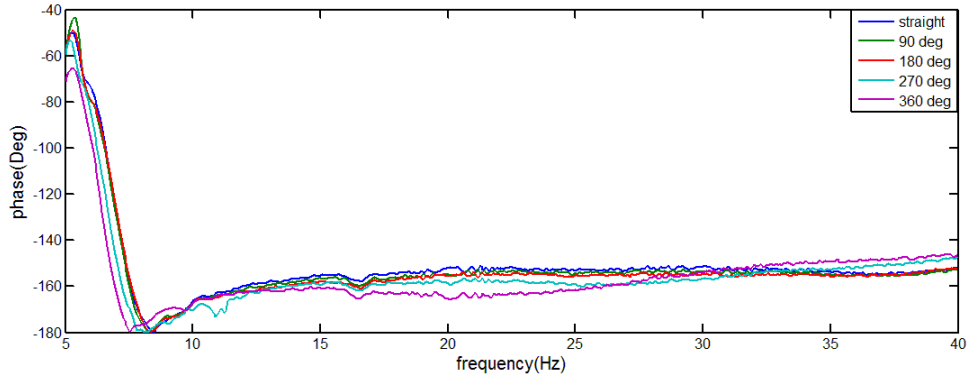

Figure 3-13: Phase of pressure and acceleration

3.5. Studying the results of testing 0.5” diameter pipe with applying different amplitudes and frequencies

A 0.5” inner diameter pipe was used to observe the frequency response of pressure gradient when the amplitude changes. The graph comparing different amplitudes is depicted in Figure (3-14). To start the test, the shaker is programmed to perform in sinusoidal harmonic movement in the range 5 to 40 Hz with a time rating of 1 second per hertz. As shown in the graph, increasing the amplitude from 0.2 mm to 0.5 mm makes a big difference in the peak value of frequency response. For instance, at 0.2 mm amplitude the highest value of the pressure gradient is nearly 6 kPa occurring around 12 Hz, but at 0.5 mm amplitude of excitation, it jumps to 40 kPa. Although they have different pick values, resonances are happening in the same frequency for both. As shown in White [21], the pressure differentiation between the entrance and exit of the pipe, ΔP and flow of water inside the pipe, Q have a relationship as $\Delta P \propto Q^2$. The experimental results can be validated, considering the fact that by increasing the amplitude of excitation, the volume of fluid passing through the pipe is increased.

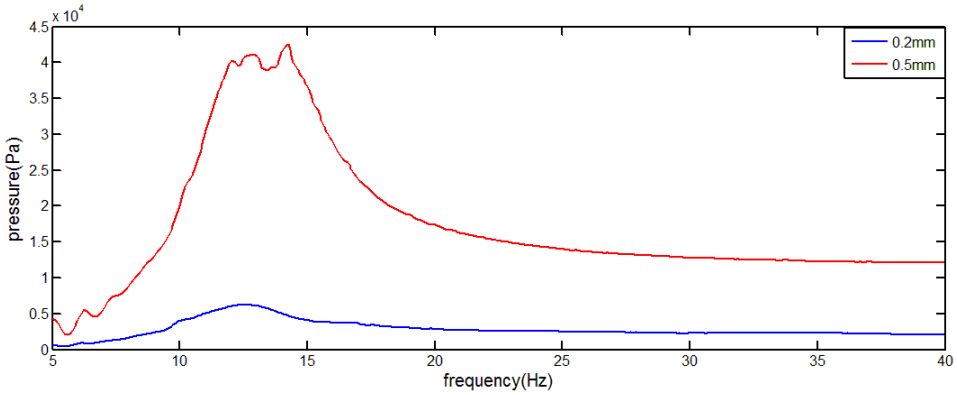

Figure 3-14: Pressure vs. frequency for different amplitude of excitation

The phase of the system between pressure and the acceleration of the shaker is depicted in Figure (3-15); it shows that the phase starts from zero and increases to -180 degree, which agrees with results from Womersley [45]; when the speed of the flow inside the pipe in reciprocating movement exceeds 10 Hz, flow lags the pressure gradient by about 90 degree .Because flow and acceleration have another 90 degree

difference in phase, the results of the phase could be approved. Another result observed from the graph concerns different amplitudes; phase between pressure and acceleration of flow of the fluid inside the pipe, does not change. It should be mentioned that to achieve a better observation of attitude of fluid inside inertia track of hydraulic engine mount, the second test apparatus has been employed. In chapter five, the second test apparatus will be explained in details.

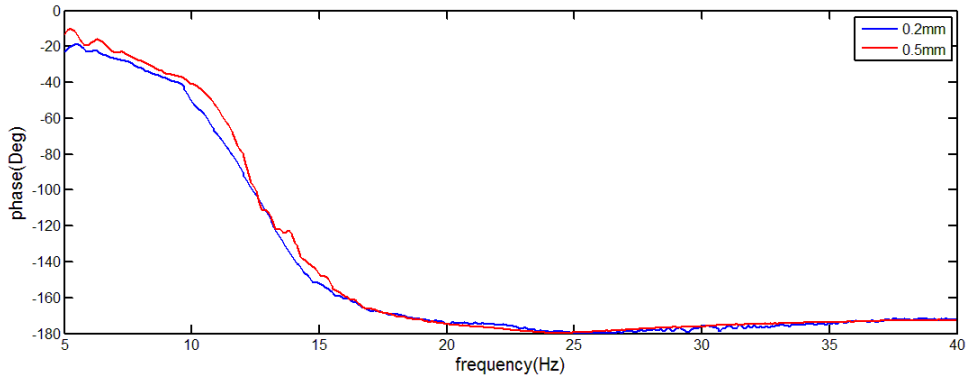

Figure 3-15: Phase lag between pressure and acceleration of flow

3.6. Conclusion

By studying the experiments explained in this chapter, we have visual information about the effects of changing some physical parameters of the pipe. The different diameter, roughness's and amplitude of the sinusoidal movement, each have their own importance in modelling the attitude of fluid that flows through a pipe under sinusoidal or harmonic reciprocating excitation. Because flow is going back and forth through the pipe, amplitude of movement affects the output pressure more than other geometrical changes. In all the fluid mechanic equations, the diameter of the pipe is a main concern; increasing or decreasing it affects the speed and flow and pressure profile. Moody [46] shows in his well-known chart that in turbulent flow, $\Delta P \propto \frac{1}{D}$ .The same property of the dynamics of fluid has been monitored when a different roughness was applied.These consequences emerge not only in the peak value of pressure differentials, but also in phase angles. Other parameters concerned with the behaviour of the dynamics of fluid

are length of the pipe and cross sectional shape of the pipe. Also, although the different angles of rotation did not show differences in pressure differential or phase lag, it should be mentioned that short pipe, with small diameter and curvature up to 360 degree has been used in our experiments. The reason for avoiding more curvature and larger pipes is to simulate the situation close to the inertia track of the engine mount. On the other hand, in other applications where rotation occurs a few times, and sizes of pipes are larger; even with higher frequency excitation, the angle of rotation may play a big role in the behaviour of fluid through the pipe.

4. An insight into modelling the resistance of the inertia track of an engine mount

This chapter is an insight to the modelling of resistance of inertia track, when fluid flows through it, under pulsatile and reciprocating excitation. The Mechanics and regime of fluid inside the inertia track has been investigated. The main equations of pressure gradient and the resistance of fluid inside a pipe along with dimensionless numbers of flow have been reviewed. The pressure gradient of fluid inside inertia track in laminar and turbulent flow has been achieved.

4.1. Mechanics of fluid

Resistance is an important factor in the mechanics of fluid being studied by many researchers using different material fluids under various situations and conditions. Before analysing the modelling of resistance of fluid inside the inertia track, some fundamental equations have been introduced and discussed. In upcoming sections the dynamics of fluid behaviour have been investigated in more detail.

4.1.1. Reynolds number

One of the most important dimensionless factors in the mechanics of fluid is the Reynolds number, used to identify the ratio of internal forces to viscous forces [21]. This number is used to define the attitudes of fluid in terms of laminar or turbulent behaviour. Researchers evaluate the Reynolds number of motion to anticipate the profile of velocity and forces and generally to determine the dynamics of fluid in all cases of study. For this project where flow inside the inertia track is concerned, the Reynolds number is defined as

$$Re = \frac{\rho V D}{\mu} = \frac{QD}{\nu A} \quad \text{4-1}$$

where ρ is the density of the fluid and V is the mean velocity of fluid inside the pipe, while Q denotes volumetric flow rate, A and D are cross sectional area and the diameter of a pipe. Also, μ is the dynamic viscosity of the fluid, and ν is the kinematic viscosity ($\boldsymbol{\nu = \frac{\mu}{\rho}}$).

4.1.2. Laminar flow

To define the laminar flow, the Reynolds number has been employed such that for Reynolds numbers lower than 2300, the regime of fluid is laminar with smooth, steady and parallel layers of fluid [44]. There are a few equations to quantify the pressure drop in a pipe when fluid is passing through it, and here, some of the more practical equations are reviewed.

4.1.3. Hagen–Poiseuille equation

In calculating fluid dynamics, Hagen-Poiseuille equations widely used in many cases, defined as

$$\Delta P = \frac{128 \mu L Q}{\pi D^4} \quad \text{4-2}$$

These parameters have the same definition as explained before along with ΔP as pressure gradient. It should be noted that there are some assumptions to derive this equation; for instance, the working fluid is a viscous fluid and incompressible while the motion inside the pipe is laminar with no acceleration. This formula is also written for a long pipe, and entrance loss has been neglected. The Hagen-Poiseuille equation has been derived from the Navier–Stokes equation.

4.1.4. Darcy–Weisbach equation

Darcy and Weisbach have done excellent research on the head loss of a pipe when laminar fluid flows through it [21]. Based on their fundamental equation, the pressure drop or head loss in pipe is related to length, diameter, and average velocity of fluid, gravity, and Darcy friction factor.

$$h_f = f_D \frac{L}{D} \frac{V^2}{2g} \qquad 4\text{-}3$$

In the mechanics of fluid, the Darcy friction factor is defined as

$$f = \frac{64}{Re} \qquad 4\text{-}4$$

In some applications, the Fanning friction factor has been used which is

$$f = \frac{16}{Re} \qquad 4\text{-}5$$

4.1.5. Turbulent flow

Turbulent flow is studied in this section as a main regime of fluid inside the inertia track. The Hagen-Poiseuille law loses its validity when the Reynolds number exceeds a certain value. Experiments show that irregular velocity fluctuations set in, causing an intensive intermixing of the various layers in the flow [47]. The profiles of the time-averaged velocity increase and the wall shear stress increases. The pressure drop no longer is proportional to $\dot{Q}$, but approximately to $\dot{Q}^2$, and the flow is then called turbulent [47]. Turbulent flow occurs at high Reynolds numbers, mostly higher than 4,000, and is dominated by inertial forces, which tend to produce chaotic eddies, vortices and other flow instabilities. Analyzing the regime and profile of velocity and pressure in turbulent

flow is more complicated than for laminar flow. It should be noticed that in the range of *2300< Re <4000*, fluid is considered transient flow which is the region that laminar flow becomes turbulent. Some efforts have been taken to identify the pressure drop of the fluid inside the pipe, and its friction factors. Here some equations are discussed.

One of the most important equations for identifying the pressure drop used for both laminar and turbulent regimes was given by White [21]:

$$\Delta P = f\frac{8L\rho}{\pi^2 D^5}Q^2 + k\frac{8\rho}{\pi D^4}Q^2 \qquad 4\text{-}6$$

Where f, is a friction factor as a function of Reynolds number and roughness, and k is the entrance loss that depends on the diameter of the pipe.

This equation shows that pressure differentiation inside the long pipe is changing linearly with the square of volumetric fluid flow. For laminar regimes, the friction coefficient is being calculated as shown, and for turbulent regimes, it is obtained by a different method which will be discussed in this section.

Blasius [44] has determined resistance of fluid in turbulent regime as

$$C_f \sim \frac{0.0791}{Re_{D_h}^{\frac{1}{4}}} \qquad 4\text{-}7$$

where C_f is the friction coefficient and D_h is the modified diameter found from

$$D_h = \frac{4A}{P} = 4 * \frac{Area}{wetted\ perimeter} \qquad 4\text{-}8$$

This can be applied for the situation where the Reynolds number is greater than 4000. But the most reliable diagram to estimate pressure gradient and friction factor was

developed by Moody [46]. He provided the chart, known as the Moody chart, to define the pressure drop with respect to Reynolds number and roughness of a pipe or tube. When using the Moody chart, researchers should be careful about the friction factor that has been used in laminar regime. Depending on the version, it would be either a Darcy or a Fanning friction factor.

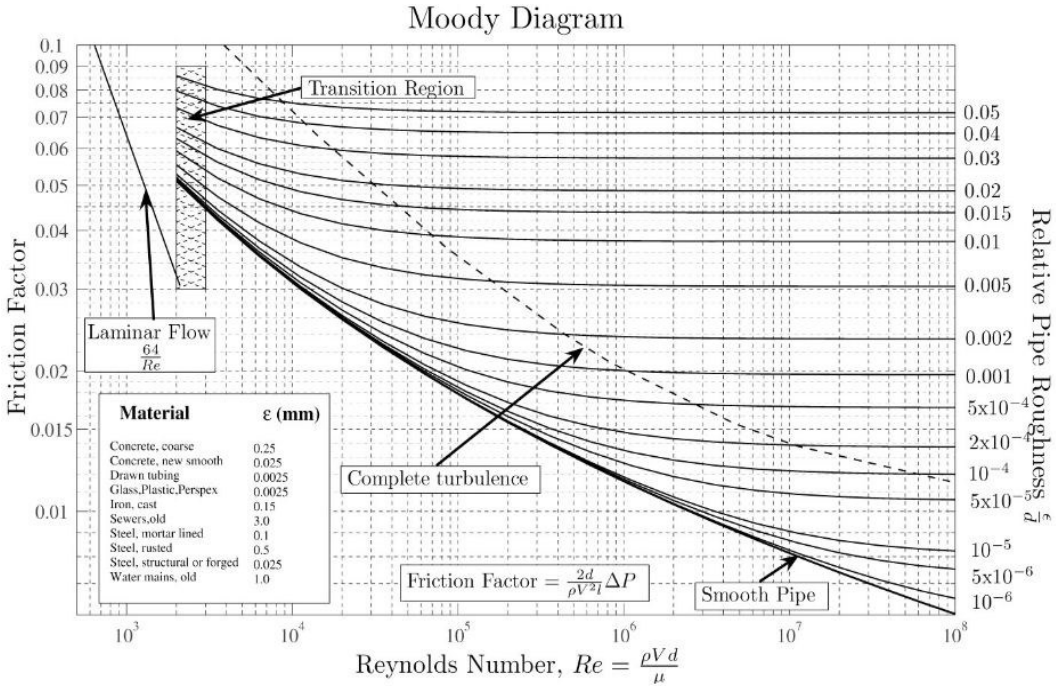

Figure 4-1: Moody diagram [46]

The chart in Figure (4-1), shows the relationship between Reynolds number and pipe friction. Calculation of friction factors depends on the type of flow encountered. Most commercial applications involve turbulent flow; in these cases, the inner roughness of the pipe has a significant effect on the friction factor. The relative roughness is the inner roughness divided by the internal diameter of the pipe. The friction factor is found by plotting the intersection of Reynolds number and relative roughness, and reading the friction factor on the left hand axis of the chart.

Studying of the Moody diagram shows that based on the Darcy-Weisbach, the friction factor can be calculated as below:

$$f = \frac{h}{\frac{l}{D}\frac{V^2}{2g}} \qquad 4\text{-}9$$

To find the pressure drop from a Moody chart, we can employ the equation of Darcy-Weisbach [47] as

$$\Delta P = f_D \frac{L}{D}\frac{\rho V^2}{2} \qquad 4\text{-}10$$

In equations 4-9 and 4-10, h denotes head loss, f is friction factor, L is length of pipe work, D is inner diameter of a pipe. V is the velocity of fluid, and g is acceleration due to the gravity. Also, there are some additional calculation have been done by Colebrook [48] and Haaland [44] to achieve the friction factor by correlation, those are independent of head loss and pressure drop.

Colebrook got the implicit equation based on Reynolds number, using ε as the factor of roughness which is

$$\frac{1}{\sqrt{f}} = -2log\left(\frac{\varepsilon}{3.7D_h} + \frac{2.51}{Re\sqrt{f}}\right) \qquad 4\text{-}11$$

But Haaland found the explicit equation also by correlation

$$\frac{1}{\sqrt{f_D}} = -1.8\,log\left(\left(\frac{\frac{\varepsilon}{D}}{3.7}\right)^{1.11} + \frac{6.9}{Re}\right) \qquad 4\text{-}12$$

Based on studies on resistance inside the pipe, we found that in turbulent flow:

- Resistance is not constant(R changes with flow)

- Pressure is proportional to approximately (flow rate) ^2
- Greater resistance when flow is turbulent, everything else remains constant
- Pressure is proportional to the 5th power of radius (i.e. Darcy-Weisbach equation)
- Turbulent flow occurs at Reynolds number greater than 4000

After reviewing the fundamentals and some practical equations of fluid flow and resistance, we will focus on the inertia track, our main concern in the thesis. As our application consists of oscillatory reciprocating flow, it is important to consider that Reynolds number is changing by direction of flow. So it is going from laminar to turbulent range, then zero, and again laminar and turbulent continuously. For this reason, none of the equations above give us accurate results for resistance inside the inertia track. In addition, in pulsatile flow, instead of using Reynolds number, kinetic Reynolds number has been used which will be introduced in the next section.

4.2. Studying the model of resistance inside inertia track

Pulsatile flow inside a pipe under the effects of periodic pressure fluctuations is a problem that has been investigated by researchers using experimental and analytical studies. It has been applied for many years in the studies of the circulation system of blood and in super-charging systems of reciprocating engines. Richardson and Tyler (1929) [47] were the first researchers whose measurements results showed that maximum axial velocity in an oscillatory flow with fast speed occurs near the wall of the pipe; it is called the “annular effect”. They worked on the sound waves in resonators. The theoretical verification of this phenomenon was made by Sexl (1930) [50] who calculated the velocity distribution. Both sinusoidal and non-sinusoidal motions of a fully developed incompressible laminar oscillatory flow in a pipe were analyzed by Womersley (1950) [45].Uchida (1959) performed an exact solution of pulsating laminar flow superimposed on the steady motion in a circular pipe under the assumption of flow parallel to the axis of the pipe[52]. He used Hagen-Poiseulle’s law on the steady

component of pressure gradient. He also presented the relation between mean mass-flow and the necessary gradient of pressure and loss of energy by dissipation that must be overcome by the excess work from the exterior.

A few researchers have investigated frictional losses in a reciprocating pipe flow. Although they gathered some data on pressure drops and on heat transfer in a tube and packed tube under reversing flow condition with high speed, they could not find frequency dependence in either pressure drop or heat transfer data. The data obtained by Taylor and Aghili [58] (1984) indicate an increase of friction coefficient over a unidirectional steady flow of water in a pipe of finite length under the effects of oscillation. Zhao and Cheng [53] found an analytical and experimental solution to pressure drop in a fully-developed laminar incompressible reciprocating pipe flow. They showed that instantaneous and cycle-average friction coefficients of this kind of flow depend not only on the kinetic Reynolds number($Re_\omega = \frac{\omega D^2}{\nu}$), but also on the dimensionless oscillation amplitude of fluid($A_0 = \frac{2u_{max}}{\omega D}$), while dimensionless axial velocity profiles of fully-developed flow, u depend only on the kinetic Reynolds number($Re_\omega = \frac{\omega D^2}{\nu}$). The process of derivation used in next section is achieved from analyzes done by Zhao and Cheng [51].

4.3. Mathematical modelling

Considering reciprocating flow inside a pipe, as an incompressible fully-developed flow, conservation equations of mass and momentum are

$$\frac{\partial u}{\partial x} = 0 \qquad 4\text{-}13$$

$$\frac{\partial u}{\partial t} = -\frac{1}{\rho}\frac{\partial P}{\partial x} + \nu\left(\frac{\partial^2 u}{\partial r^2} + \frac{1}{r}\frac{\partial u}{\partial r}\right) \qquad 4\text{-}14$$

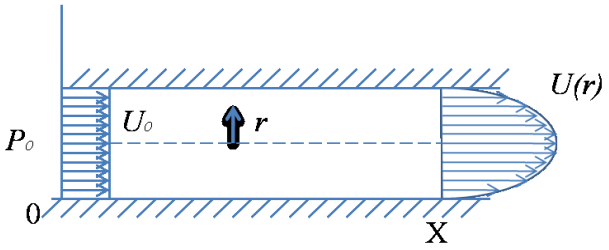

Figure 4-2: Schematic of flow inside a pipe

where r and $x$are the radial and axial coordinates, ρ and $\nu$are the density and the kinematic viscosity of fluid, u is velocity and P is the pressure of the fluid. Assuming the reciprocation of flow is caused by a sinusoidal varying pressure gradient defined as

$$\frac{1}{\rho}\frac{\partial P}{\partial x} = k\cos\omega t \qquad 4\text{-}15$$

Whereω and k are circular frequency and amplitude of oscillation of motion. Zhao and Cheng [51] achieved the exact solution for the axial velocity profile of a fully-developed reciprocating flow, obtained by modifying Uchida's analytical solution [52], which is

$$u = \frac{kD^2}{4\alpha^2\nu}\left[B\cos\omega t + (1-A)\sin\omega t\right] \qquad 4\text{-}16$$

$A$and$B$are achieved respectively from

$$A = \frac{ber\,\alpha\; bei\; 2\alpha R + bei\,\alpha\; ber\; 2\alpha R}{ber^2\alpha + bei^2\alpha} \qquad 4\text{-}17$$

$$B = \frac{ber\,\alpha\; ber\; 2\alpha R - bei\,\alpha\; bei\; 2\alpha R}{ber^2\alpha + bei^2\alpha} \qquad 4\text{-}18$$

$ber\,\alpha$ and $bei\,\alpha$ are Kelvin functions defined as real and imaginary parts of $J(\alpha e^{\frac{3\pi i}{4}})$, and J is a Bessel function of first kind and is clarified as

$$ber\ \ (z) = Real\left[J\ \ \left(ze^{\frac{3\pi i}{4}}\right)\right] = 1 + \sum_{n=1}^{\infty} \frac{-1^n(\frac{1}{2}z)^{4n}}{[(2n)!]^2} \qquad 4\text{-}19$$

$$bei\ \ (z) = imag\left[J\ \ \left(ze^{\frac{3\pi i}{4}}\right)\right] = \sum_{n=0}^{\infty} \frac{-1^n(\frac{1}{2}z)^{2+4n}}{[(2n+1)!]^2} \qquad 4\text{-}20$$

with $R\left(\frac{r}{D}\right)$ is the dimensionless radial coordinate, and with α denoting Womersley number defined by

$$\alpha = \frac{D}{2}\sqrt{\frac{\omega}{\nu}} = \frac{1}{2}\sqrt{Re_\omega} \qquad 4\text{-}21$$

As stated already, $Re_\omega = \frac{\omega D^2}{\nu}$ is the kinetic Reynolds number which has same effect as regular Reynolds number in a unidirectional steady flow [53]. If integration over the cross sectional area of the pipe is applied to equation (4-16), the following exact expression for the mean velocity yields:

$$u_m\ = u_{max}\sin\phi \qquad 4\text{-}22$$

Where u_{max} is the maximum speed of fluid and ϕ, is the phase shift between velocity and externally imposed pressure gradient, defined to be

$$u_{max} = \frac{kD^2\sigma}{32\nu} \qquad 4\text{-}23$$

$$\phi = \frac{\pi}{2}(\omega t - \Lambda) \qquad 4\text{-}24$$

With

$$\sigma = \frac{8}{\alpha^3}\sqrt{(\alpha - 2C_1)^2 + 4C_2^2} \qquad 4\text{-}25$$

And

$$\Lambda = tan^{-1}\frac{(\alpha - 2C_1)}{2C_2} \qquad 4\text{-}26$$

where $C_1$and C_2 are achieved from

$$C_1 = \frac{ber\ \alpha\ bei'\alpha - bei\ \alpha\ ber'\ \alpha}{ber^2\alpha + bei^2\alpha} \qquad 4\text{-}27$$

$$C_2 = \frac{ber\ \alpha\ ber'\alpha + bei\ \alpha\ bei'\ \alpha}{ber^2\alpha + bei^2\alpha} \qquad 4\text{-}28$$

with $ber'\alpha = \frac{d(ber\ \alpha)}{d\alpha}$ and $bei'\alpha = \frac{d(bei\ \alpha)}{d\alpha}$; so dimensionless axial velocity for reciprocating flow $\left(U = \frac{u}{u_{max}}\right)$ depends on $R, \tau$and Re_ω, where $\tau = \omega t$ is the dimensionless time related to the phase angle ϕ as $\tau = 2(i-1)\pi + \phi$ with i as the number of turns. These equations prove the fact that the dimensionless axial velocity of fully-developed flow, at a known time and position, is only a function of kinetic Reynolds number. The instantaneous and cycle average friction coefficients of a reciprocating flow has been clarified as

$$c_{f,\infty} = \frac{\tau_w(\tau)}{\frac{1}{2}\rho u_{max}^2} = \frac{\mu\left(\frac{\partial u}{\partial r}\right)_{r=\frac{D}{2}}}{\frac{1}{2}\rho u_{max}^2} \quad \text{4-29}$$

$$\bar{c}_{f,\infty} = \frac{1}{2\pi}\int_0^{2\pi} |\, c_{f,\infty}(\tau)| d\tau \quad \text{4-30}$$

In the equation 4-29, τ_w is the shear stress of the wall of the pipe. Deriving the differentiation of equation (4-16) and substituting in equations (4-29) and (4-30) leads us to the exact expression for friction coefficient of fully-developed reciprocating flow

$$c_{f,\infty} = \frac{32F_\omega}{A_0}\, sin(\phi + \phi_1) \quad \text{4-31}$$

and

$$\bar{c}_{f,\infty} = \frac{64F_\omega}{\pi A_0} \quad \text{4-32}$$

where

$$F_\omega = \frac{\sqrt{C_1^2 + C_2^2}}{16\sqrt{(\alpha - 2C_1)^2 + 4C_2}} \quad \text{4-33}$$

$$\phi_1 = tan^{-1}[\frac{(\alpha - 2C_1)}{2C_2}] - tan^{-1}[\frac{C_2}{C_1}] \quad \text{4-34}$$

$$A_0 = \frac{2u_{max}}{\omega D} \qquad 4\text{-}35$$

where $\phi_1$denotes phase angle difference in degrees between the wall shearing stress and cross-sectional mean velocity u_m defined in equation (4-22) . Also, A_0 is a dimensionless fluid displacement which can be explained on the other hand as

$$u_{max} = \frac{x_{max}\omega}{2} \qquad 4\text{-}36$$

Then

$$A_0 = \frac{x_{max}}{D} \qquad 4\text{-}37$$

where x_{max}, as the maximum bulk fluid displacement. It also has been found that in laminar flow, the approximate correlation equation for prediction of the cycle-averaged friction coefficient is [54]:

$$\bar{c}_{f,l} = \frac{3.27192}{A_0\left(Re_\omega^{0.548} - 2.03946\right)} \qquad 4\text{-}38$$

By looking at the instantaneous friction coefficient more deeply, we observe that this value can be negative or positive depending on the direction of fluid flow inside the pipe. To derive the equation which matches the inertia track of the engine mount, we should return to momentum equation (4-14), and after multiplying both sides by $2\pi r dr$,integration over cross sectional area and then the length of pipe from *x=0* to *x=L*, have been applied, yielding

$$\frac{\Delta P}{L} = \rho \frac{du_m}{dt} + \frac{4\tau_\omega}{D} \qquad 4\text{-}39$$

$$\Delta P = I_i \dot{Q}_\iota + \frac{4L}{D}\tau_w$$

Where I_i is inertia of the fluid inside the inertia track defined as

$$I_i = \frac{m}{A^2} = \frac{\rho v}{\left(\frac{\pi D^2}{4}\right)^2} = \frac{4\rho L}{\pi D^2} \qquad 4\text{-}40$$

As m denotes mass of the fluid and Athe cross sectional area of the pipe, from equations (4-29) and (4-31), we can replace $\tau_w$and $c_{f,\infty}$, and considering $Q_{max} = u_{max}A$, we obtain

$$\Delta P = \frac{\rho L}{A}\dot{Q}_i + \frac{32L\rho F_\omega}{A}\omega Q_{max} sin(\phi + \phi_1) \qquad 4\text{-}41$$

To obtain the instantaneous fluid flow and its derivative in equation (4-41), $\sin(\phi + \phi_1)$ is expanded and yields

$$\Delta P = \frac{\rho L}{A}\dot{Q}_i + \frac{32L\rho F_\omega}{A}\omega Q_{max}\ [sin(\phi)\, cos(\phi_1) + cos(\phi) sin(\phi_1)] \qquad 4\text{-}42$$

Then if we return to equation (4-22) ($u_m = u_{max}\, sin\, \phi$) and multiply both sides in the cross sectional area of pipe we will find the instantaneous flow Q_i as follows

$$Q_i = Q_{max}\sin\phi \qquad 4\text{-}43$$

Then

$$\Delta P = \frac{\rho L}{A}\dot{Q}_i + \frac{32L\rho F_\omega}{A}\omega Q_i \cos(\phi_1) + \frac{32L\rho F_\omega}{A}\sin(\phi_1)\omega Q_{max}\cos(\phi) \qquad 4\text{-}44$$

By looking at equation (4-44) more deeply, we find the derivative of flow rate $(\dot{Q}_i)$ with respect to time which is $(\omega Q_{max}\cos\phi)$; finally; we achieve the following equation

$$\Delta P = (\frac{\rho L}{A} + \frac{32L\rho F_\omega}{A}\sin(\phi_1))\dot{Q}_i + (\frac{32L\rho F_\omega}{A}\omega\cos(\phi_1))\,Q_i \qquad 4\text{-}45$$

All the parameters can be calculated using the previous equations, and obtaining the pressure differentiation of fluid flows inside the inertia track of the engine mount is achievable. In the next section the gathering of experimental data and implementing them inside the formula is studied.

It should be noted that all the above equations are based on the assumption that flow is laminar and they are valid in the range of $23 \leq Re_\omega \leq 395$ and $0 \leq A_0 \leq 26.4$; however at a higher speeds of fluid movement with a different diameter of tube, we may reach turbulent flow. For instance, in a situation where $81 \leq Re_\omega \leq 540$ and $53.4 \leq A_0 \leq 113.5$, it was found that the following algebraic equation can predict the friction coefficient of cyclically turbulent oscillatory flow [54]

$$\bar{c}_{f,t} = \frac{1}{A_0}(\frac{76.6}{Re_\omega^{1.2}} + 0.40624) \qquad 4\text{-}46$$

To achieve the pressure differential of fluid in two heads of a pipe, under oscillatory excitation, application of the same method used to obtain equation (4-45), yields

$$\Delta P = \left(\frac{\rho L}{A} + \frac{LB\rho\pi}{2A}\sin(\phi_1)\right)\dot{Q}_i + \left(\frac{LB\rho\pi}{2A}\omega\cos(\phi_1)\right)Q_i \quad \text{4-47}$$

with

$$B = \left(\frac{76.6}{Re_\omega^{1.2}} + 0.40624\right) \quad \text{4-48}$$

4.4. Evaluating the cycle average friction coefficient

To study the cycle average friction coefficient at different amplitudes of excitation under sinusoidal movement, equation (4-38) has been evaluated in Figure (4-3).

$$\bar{c}_{f,l} = \frac{3.27192}{A_0\left(Re_\omega^{0.548} - 2.03946\right)} \quad \text{4-38}$$

In this case of study, the amounts of cycle average resistance at frequency range of 5 to 40 Hz with amplitudes of 0.5, 1 and 2 mm have been calculated. A_0 and Re_ω have been obtained and implemented in equation (4-38).As observed from the Figure (4-3), the higher amplitude causes a lower cycle average friction coefficient inside the inertia track, and this value will decrease by increasing the frequency of oscillation. The reduction of resistance is occurring faster before the frequency of 10 Hz, while the incline of the graph is larger in this range of frequency. Although the friction decreases at higher amplitude of excitations, they all have the same trend with greater slope until 10 Hz, slowly decreasing after that frequency. In addition, it can be shown that the resistance has frequency and amplitude dependency. To compare the resistance of reciprocating fluid under and pulsatile excitation in laminar and turbulent flow, equation (4-46) is given as

$$\bar{c}_{f,t} = \frac{1}{A_0}\left(\frac{76.6}{Re_\omega^{1.2}} + 0.40624\right) \qquad 4\text{-}46$$

Figure (4-4) shows that the amount of resistance in turbulent regime is larger than in laminar regime flow. Both laminar and turbulent resistances have the same trend with bigger slopes at lower frequencies. The dependency on frequency is reduced by increasing the frequency, and it can be observed that at higher frequencies the slopes of the graphs are near flat.

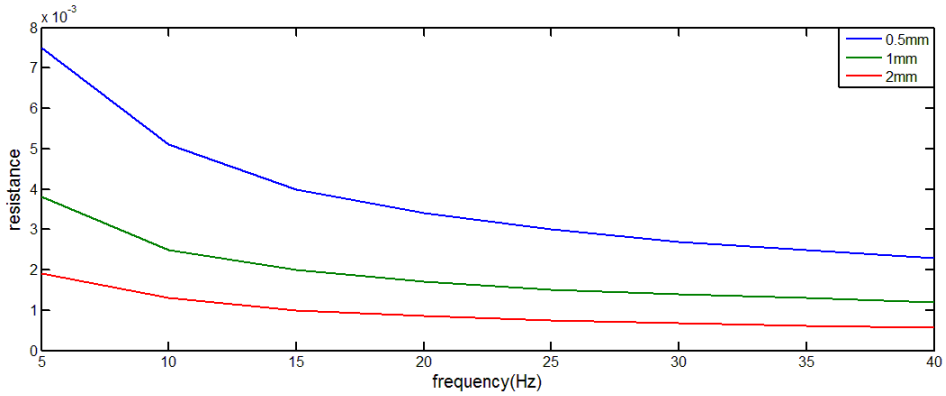

Figure 4-3: Cycle average resistance vs. frequency with different amplitude of excitation

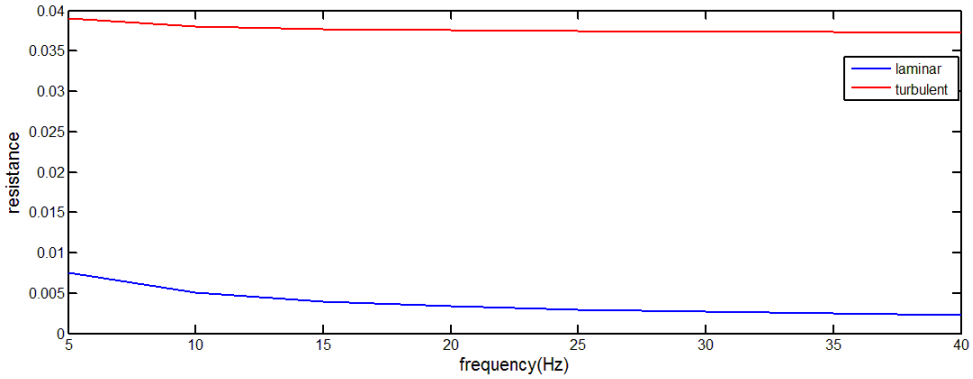

Figure 4-4: Comparison of cycle average resistance vs. frequency in laminar and turbulent regimes

4.5. Conclusion

In this chapter, the pressure drop of pulsatile and reciprocating flow inside inertia track has been investigated. By looking at equation (2-5),

$$P_1 - P_2 = I_i \dot{Q}_i + R_i Q_i \qquad 2\text{-}5$$

and comparing it with equations (4-45) and (4-47), the new model of resistance of inertia track in laminar, R_l, and turbulent flow, R_t, will be define as

$$R_l = \frac{32 L \rho F_\omega}{A} \omega \cos(\phi_1) \qquad 4\text{-}49$$

and

$$R_t = \frac{LB\rho\pi}{2A} \omega \cos(\phi_1) \qquad 4\text{-}50$$

with

$$B = \left(\frac{76.6}{Re_{\omega}^{1.2}} + 0.40624\right)$$

In the next chapter, implementing of these new resistances in HEMPP will be evaluated and results will be discussed.

5. Simulation and verification of System Models

In this chapter, simulation and verification of the system model are performed. The second test apparatus to verify the obtained equations of previous chapter is introduced in this chapter. First of all, the least square estimation method is applied to obtain the resistance of fluid inside the inertia track. This method has been used by many researchers to evaluate the resistance factor of the inertia track [17] [42]. Validation of the pressure drop equations which have been achieved in the last chapter has been investigated in the second part of this chapter. Moreover, simulation of modelling the dynamic stiffness of the engine mount to observe the effects of using different rubbers and of applying higher resistances has been studied. Final equations of new model of resistance obtained in chapter 4 have also been applied to model the dynamic stiffness of the engine mount to check progress in solving the problem.

5.1. Experimental setup

After studying the mechanics of fluid and the behaviour of fluid inside the inertia track, the thesis now quantifies equations obtained by introducing the test apparatus designed to get experimental results with best accuracy. As design criteria, the system had to be able to prove oscillatory input conditions to match those found within the mount. For this reason, two identical cylinders have been used with size similar to that of the upper and lower chamber of the engine mount. Figure (5-1), illustrates the test apparatus. Between these two cylinders we located the unit that containing the inertia track and decoupler of the engine mount that was provided by decomposing the engine mount to observe everything close to the real situation. Figure (5-2) shows a schematic of the unit. The lower piston is the location of the pressure sensor installed close to the top, just under the engine mount component. Both cylinders are filled with water, and a piston passes through the lower cylinder.

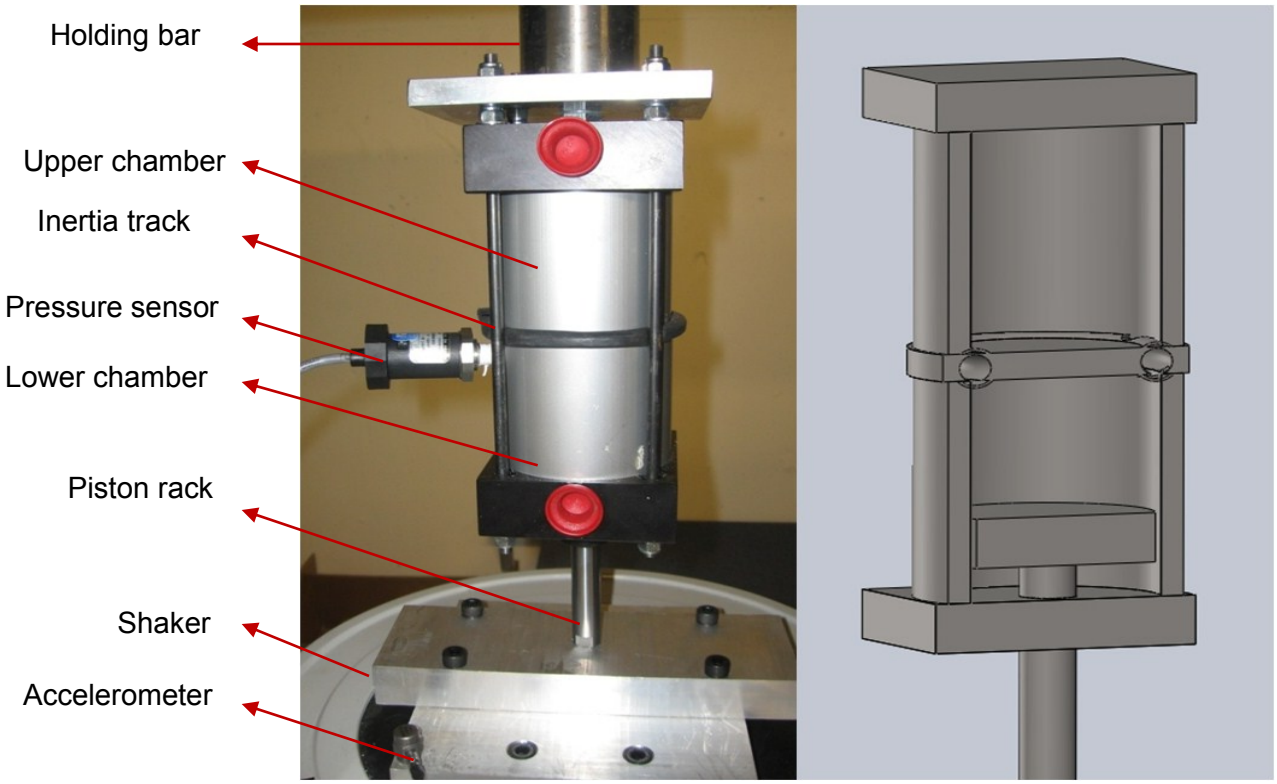

Figure 5-1: Schematic and mechanical experimental setup

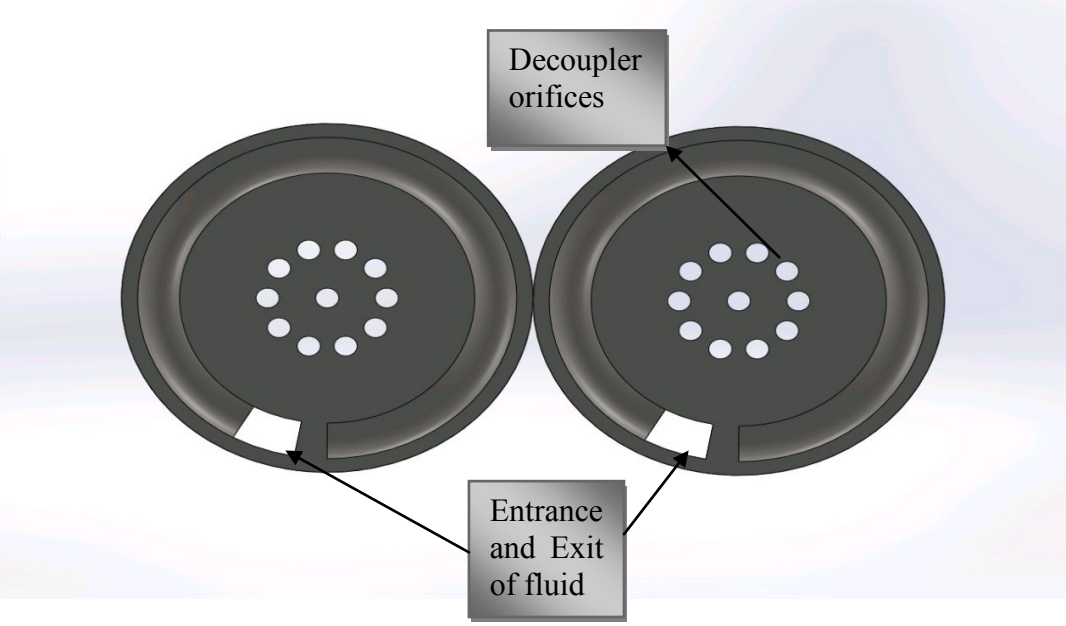

Figure 5-2: Schematic view of component of engine mount containing inertia and decoupler

The piston rack is attached to the bolted plate on the surface of the shaker, transferring the frequency-dependent motion of the shaker to the fluid inside the cylinders.

Putting the pressure sensor right under the inertia track enables us to assess the pressure of fluid entering the inertia track. Because the inertia track is being studied in this research and is the main focus, the decoupler has been blocked to make sure the inertia track is the only way to allow flow from the lower cylinder to the upper and from the upper to the lower. Finally, four bars are passed through the lower and upper caps for bolting the system and keeping all components of the apparatus locked together, preventing unwanted movement and leakage. Because the upper cylinder is full of water and open at one end, we can calculate the pressure at the other end of the inertia track very simply. Furthermore, one Dytran accelerometer has been used to close the electrical loop and provide the feedback for the shaker. The pressure sensor and accelerometer and hydro-electronic shaker are the same as those described in chapter 3. Sealing the unit should be done very precisely to avoid leakage and prevent the existence of air bubbles. Air bubbles inside the cylinders or the inertia track would cause

huge uncertainties in results by creating unnecessary compliances and may damage the pressure sensor by exceeding the pressure limit.

To start the test, the shaker has been programmed to move with sinusoidal motion in different selected frequencies and amplitudes. The whole unit should be fixed without any extra movement as a result of fixing the top with iron bar to the chassis. Lubrication of the piston is an important requirement to allow it to slip smoothly inside the cylinder and avoid additional forces in the system.

5.2. Least square estimation method

The method of least square has been used by a few researchers to find the linear and nonlinear resistance of the inertia track. Geisberger [17] and Zhang et al. [42] have used this method to achieve the resistances of the inertia track when the fluid was a mixture of water and ethylene glycol. This method is a standard approach to estimate solutions of over-determined systems in cases of having more equations than unknowns. In addition, least square means that the overall solution minimizes the sum of squares of errors made as the result of every single equation. This method is being used to minimize the difference between observed values and fitted values provided by models. Equation (2-34) has been defined for the inertia track, considering R_{i1} and R_{i2} as linear and nonlinear terms of resistance inside the inertia track. They have added the nonlinear terms to equation (2-25) which yields,

$$P_1 - P_2 = I_i\dot{Q}_i + (R_{i1} + R_{i2}|Q_i|)Q_i \qquad 2\text{-}34$$

In the matrix form of equation (2-34), the pressure difference and flux for different actuator velocities t, are assigned to ΔP^t and Q_i^t, respectively. For the series of velocities denoted by 1, 2..., n, the nonlinear and steady state momentum equations of the fluid passing through the inertia track is:

$$P = YR$$

$$P = \begin{bmatrix} \Delta P^1 \\ \Delta P^2 \\ \Delta P^3 \\ . \\ . \\ . \\ \Delta P^n \end{bmatrix}, \qquad Y = \begin{bmatrix} \dot{Q}_i^1 & |Q_i^1|Q_i^1 \\ \dot{Q}_i^2 & |Q_i^2|Q_i^2 \\ \dot{Q}_i^3 & |Q_i^3|Q_i^3 \\ . & . \\ . & . \\ . & . \\ \dot{Q}_i^n & |Q_i^n|Q_i^n \end{bmatrix} \quad \text{and} \quad R = \begin{bmatrix} I_i \\ R_{i1} \\ R_{i2} \end{bmatrix}$$

Using the least square method, therefore, we can estimate inertia and resistances, R^* as

$$R^* = (Y' * Y)^{-1} * Y' * P \qquad 5\text{-}1$$

To obtain the data for this method, an experimental setup has been used to measure the pressure of fluid flowing inside the inertia track; and knowing that the inertia track is open to the atmosphere from the other end, we can calculate the value of each parameter of matrix. The fact that the shaker is moving in a sinusoidal pattern and the piston has constant area helps us to calculate the parameter of matrix Y. To achieve the demanded values, we need to have at least three sets of equations and by using a DAC cart, we can obtain enough time domain data to estimate the inertia and resistances of the inertia track.

To start the experiment, the shaker has been programmed to run sinusoidal with constant frequency for a few seconds, and 1000 data per second have been measured. The results of inertia and linear and nonlinear resistance of the inertia track at a dwell frequency of 15 Hz are listed as

$$I_i = 9.65 * 10^5 \frac{Ns^2}{m^5}$$

$$R_{i1} = 3.13 * 10^7 \frac{Ns}{m^5}$$

$$R_{i2} = 2.46 * 10^{11} \frac{Ns^2}{m^8}$$

Figure (5-3) depicts the evaluation of the accuracy of this method by comparing with measured data the result of multiplying matrix $R^*$by matrix Y; the results agree well.

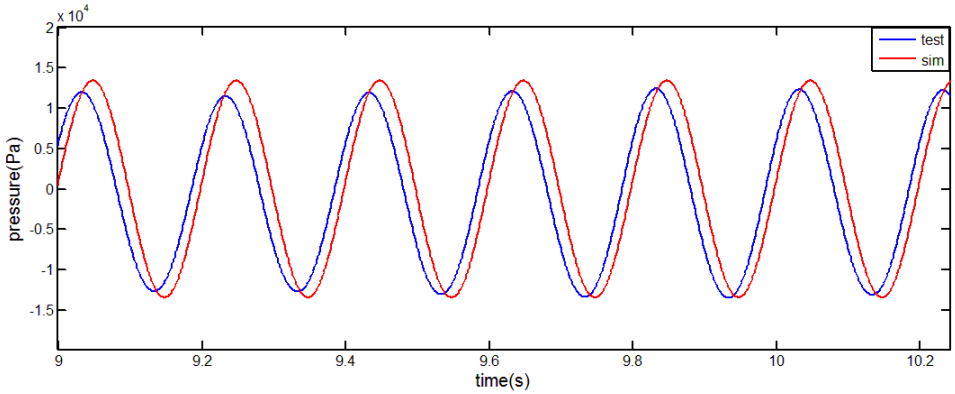

Figure 5-3: Comparison of measured and calculated pressure using least square estimation

Although this method has been used by a few researchers, it has not been reliable in this thesis. Testing different frequencies and amplitudes, as well as different numbers of measured data, to put in a MATLAB code and obtaining the required values, giving us different results each time that the discrepancy between results is not negligible. Moreover, it should be noticed that in fact, in each iteration, there are some singular matrices that are not invertible, and therefore the accuracy of this estimation is doubtful.

5.3. Verification of equations of momentum achieved for inertia track

Now the equations of pressure differentiation of the inertia track with respect to the cross sectional area of the pipe is being evaluated experimentally.

It can be seen from the equation (4-45) that all the parameters on the right side of equations are easy to calculate.L and A are length and cross sectional area of the inertia track which are known, ω represents radial frequency of oscillation, and $\rho$is the fluid density that here, density of water is used ($\rho = 1000\, kg/m^3$).Q_i and $\dot{Q}_i$ can be

obtained from speed of the actuator multiply by constant cross section of the piston and its derivative. In addition,F_ω and ϕ can be found by applying Kelvin and Bessel functions

$$\Delta P = \left(\frac{\rho L}{A} + \frac{32L\rho F_\omega}{A}\sin(\phi_1)\right)\dot{Q}_i + \left(\frac{32L\rho F_\omega}{A}\omega\cos(\phi_1)\right)Q_i \qquad 4\text{-}45$$

For collecting experimental results, the shaker has been programmed to run a sinusoidal pattern with constant frequency of oscillation. Because these equations are derived in time domain and the shaker is able to provide frequency domain data only, the high speed data acquisition system (DAC) has been used to gather the time domain outputted data from the pressure sensor, with 1000 samples observed per one second of operation.

Experimental results are being compared with analytical results in Figures (5-4) and (5-5). At 5 Hz and 10 Hz, which are the focuses here, experimental and simulation data agree very well in phase and amplitude, showing that the suggested model is a reliable equation for studying the attitude of fluid inside the inertia track.

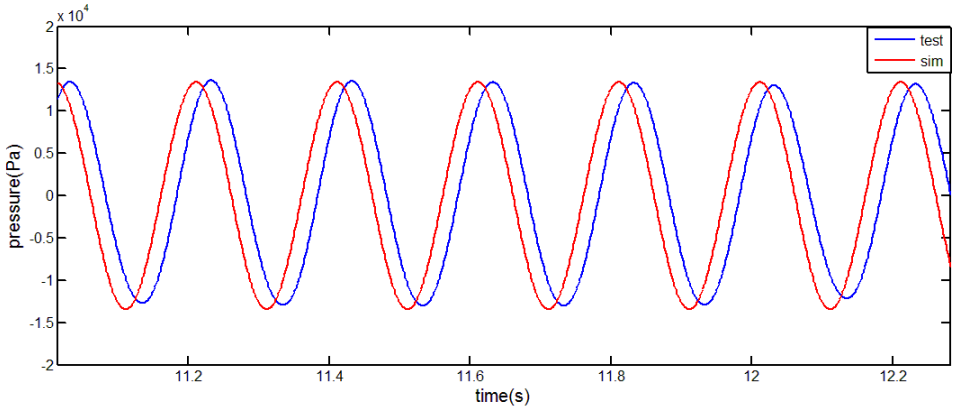

Figure 5-4: Pressure differentiation vs. time for 5 Hz

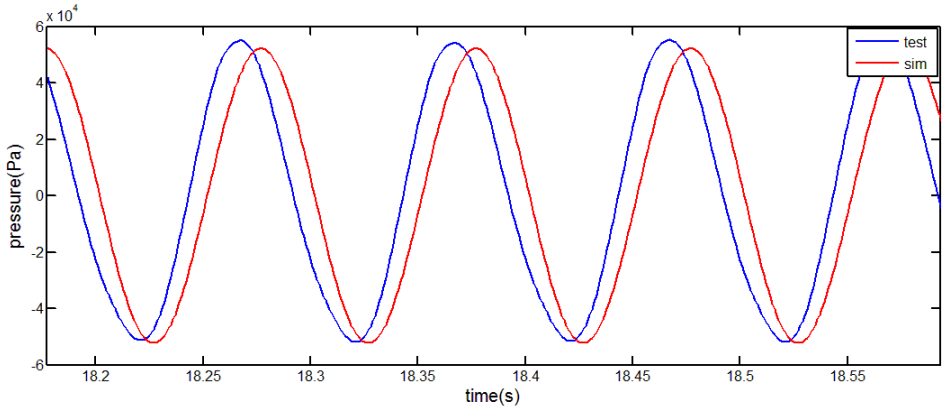

Figure 5-5: Pressure differentiation vs. time for 10 Hz

To examine the validation of equation (4-47) for turbulent regime, the same technique for checking laminar flow equation has been used; to reach the turbulent regime, the shaker should be programmed to provide the higher frequency of excitation. Figure (5-6) compares the pressure differentiations of the inertia track with the simulated model results obtained from the equation. As observed, the test and simulation agree very well. In Figure (5-7) the variation of flow versus time is depicted. The negative value of Q shows the direction of movement under sinusoidal and frequency excitations.

$$\Delta P = \left(\frac{\rho L}{A} + \frac{LB\rho\pi}{2A}\sin(\phi_1)\right)\dot{Q}_i + \left(\frac{LB\rho\pi}{2A}\omega\cos(\phi_1)\right)Q_i \qquad 4\text{-}47$$

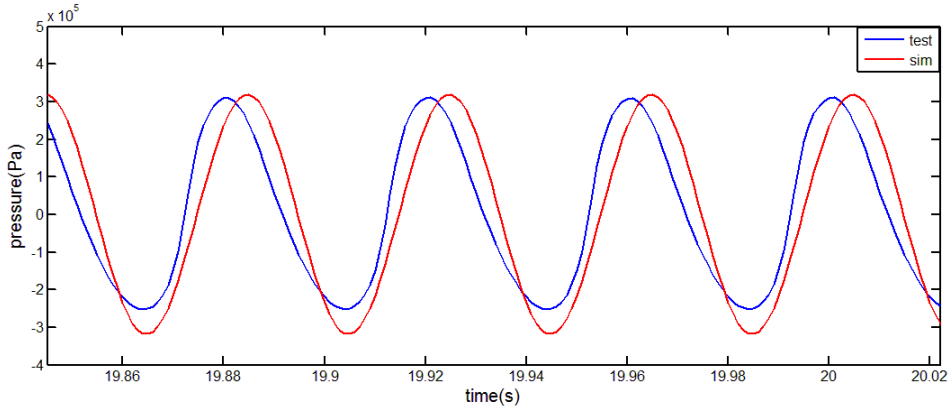

Figure 5-6: Pressure differentiation vs. time for 25 Hz

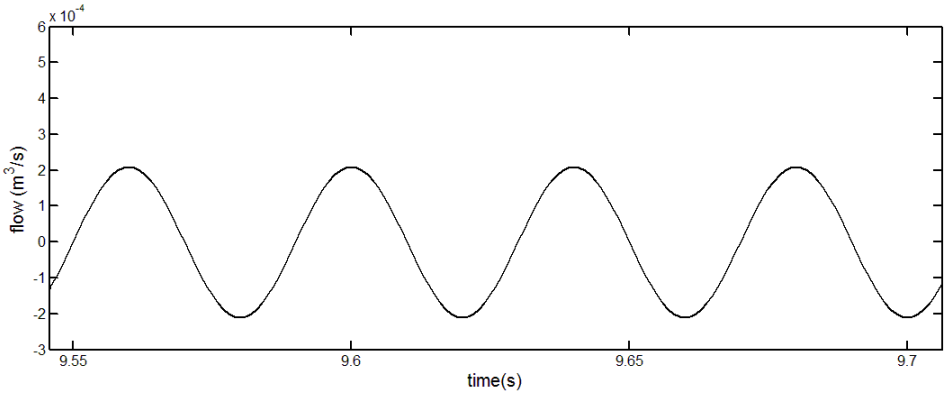

Figure 5-7: Fluid flow vs. time in frequency of 25 Hz

5.4. Prediction of dynamic stiffness of hydraulic engine mount with implantation of new model for resistance

To check the improvement of prediction of dynamic stiffness, using the new model for resistance, the first step was to rebuild the HEMPP, a program written using both the MATLAB and C++ programming languages. The entire GUI and various parameter calculations were written in C++ while all of the core mathematics in HEMPP were done in MATLAB. The rebuilding of the HEMPP was done by previous researchers using MATCOM45 Compiler. In addition, FFT has been written to convert time domain

data to frequency domain. By following the method of HEMPP to build the library files for use in simulation, they were able to generate the program in MATLAB.

At this point we needed to implement our new model of resistance inside the MATLAB codes to check the modification of HEMPP but before doing that, we will observe the effect of some materials and parameters in the simulation of dynamic stiffness.

5.4.1. The prediction of dynamic stiffness using different rubbers

In this section two types of rubber are studied to observe the dependency of dynamic stiffness to the main rubber material. 50 Duro and 45 Duro rubbers were examined to evaluate the influence of material on the stiffness K_r and damping b_r characteristics of the mount. The simulation was done by applying 1 and 2 mm amplitudes from frequencies of 2 Hz to 40 Hz. Applying geometrical parameters and running the simulation yields the results depicted in Figures (5-8), (5-9), (5-10), (5-11).

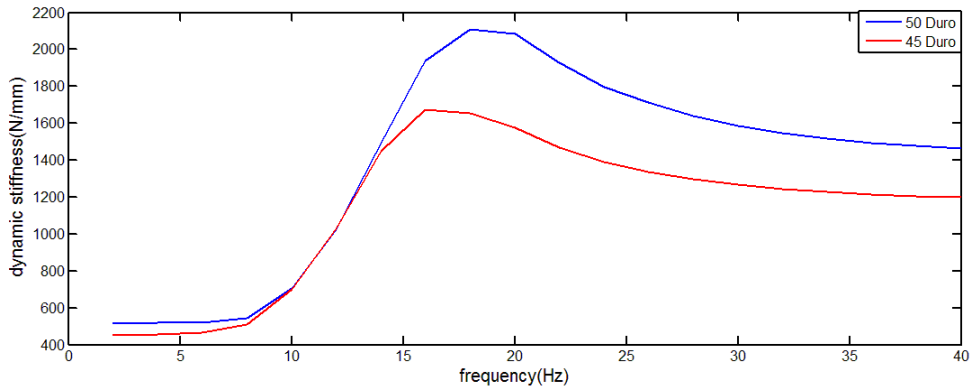

Figure 5-8: Dynamic Stiffness vs. frequency, using different rubbers with 1 mm amplitude of excitation

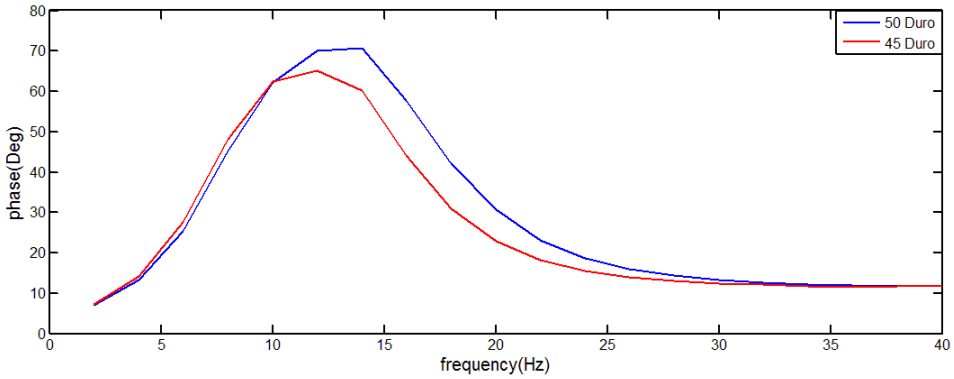

Figure 5-9: Phase vs. frequency, using different rubbers with 1 mm amplitude of excitation

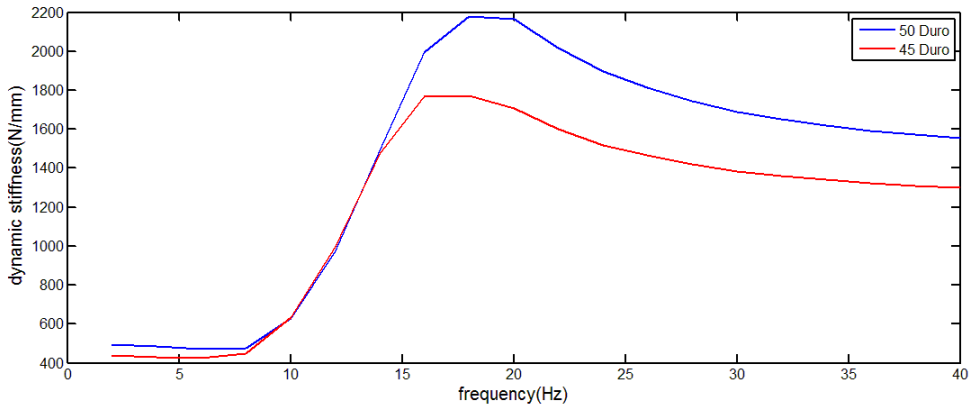

Figure 5-10: Dynamic Stiffness vs. frequency, using different rubbers with 2 mm amplitude of excitation

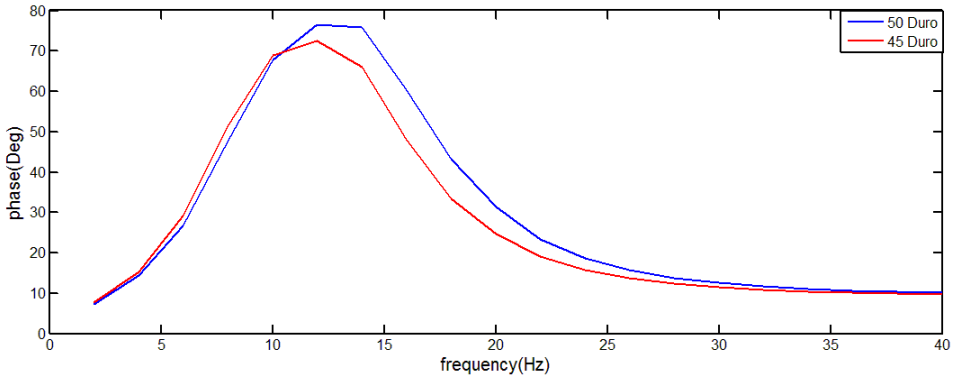

Figure 5-11: Phase vs. frequency, using different rubbers with 2 mm amplitude of excitation

Figures (5-8) and (5-9) for amplitude of 1mm in sinusoidal motion, and Figures (5-10) and (5-11) for amplitude of 2 mm show discrepancies on dynamic stiffness and phase when two different rubbers are used to build the hydraulic engine mount. The gap is obvious when the frequency is higher than 17 Hz, because of the effect of compliance of the main rubber on the whole functional characteristics of the mount.

Equation (2-33) also proves the fact that at higher frequencies C_1plays the main role in the frequency response of dynamic stiffness. Although changing the rubber has a big influence on dynamic stiffness of the mount, the effect on phase is not very obvious.

5.4.2. The prediction of dynamic stiffness, increasing the resistance of inertia track

In this section a new model of resistance is implemented inside codes and then increased by 20% and 40% to observe the effect of resistance on predicting dynamic stiffness and phase of the mount. Resistance parameter R does not alter the natural frequency of the liquid column in the inertia track. But it can change the shape of resonance and peak value of phase in both 1 mm and 2 mm amplitude of excitations. As illustrated in Figures (5-12), (5-13), (5-14), and (5-15), by increasing the resistance, the peak of dynamic stiffness curves and phase curves are reduced. On the other hand, arising resistance limits the motion of fluid inside the inertia track during resonance, causing the pressure peak to reduce and making the total system response smoother.

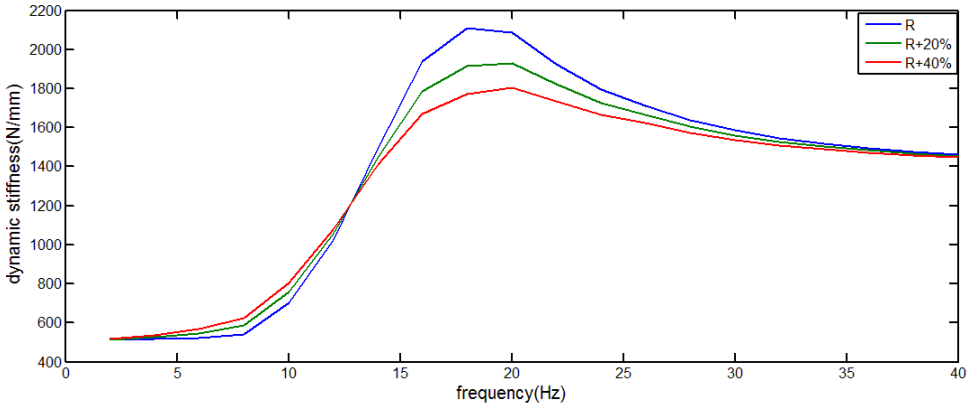

Figure 5-12: Frequency response of dynamic stiffness under the excitation of 1 mm, using different resistances

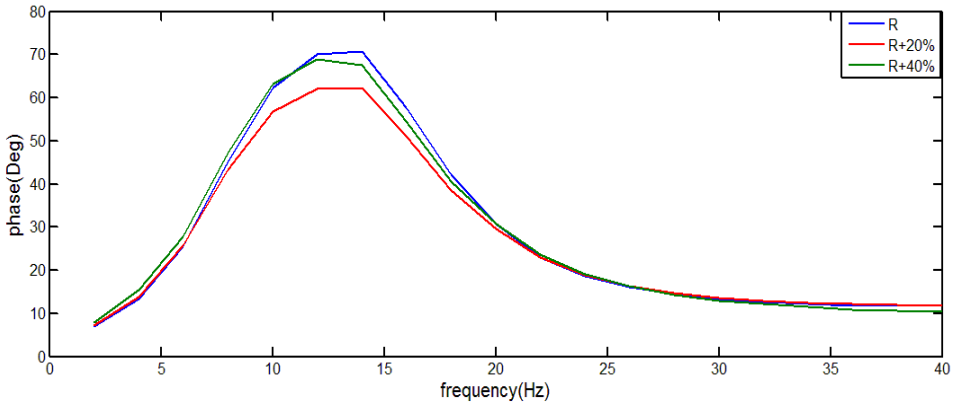

Figure 5-13: Phase vs. frequency under the excitation of 1 mm, using different resistances

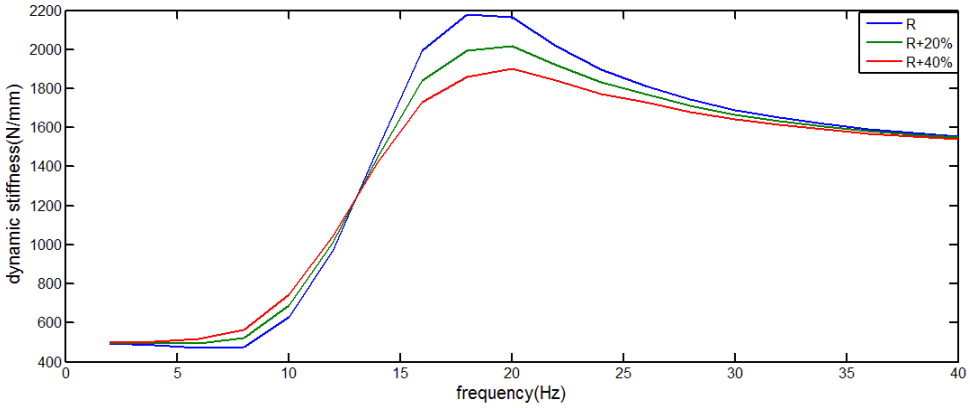

Figure 5-14: Frequency response of dynamic stiffness under the excitation of 2 mm, using different resistances

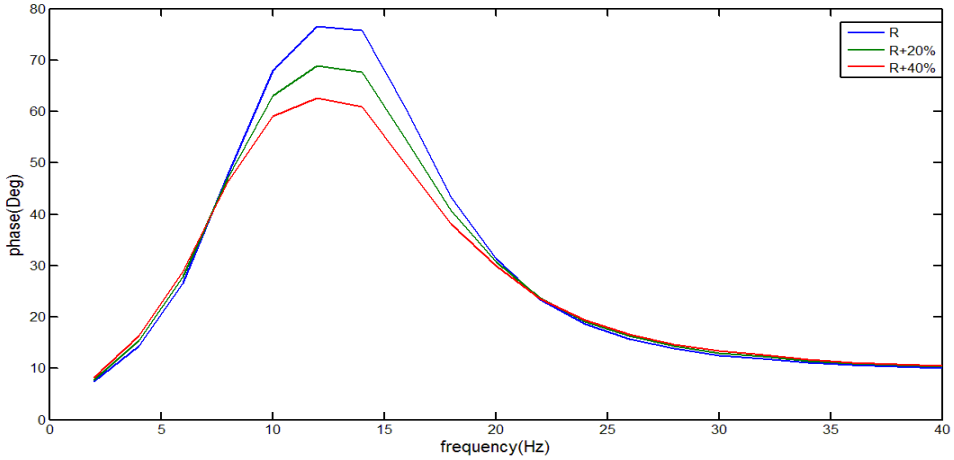

Figure 5-15: Phase vs. frequency under the excitation of 2 mm, using different resistances

5.5. Final graphical results

After the studying the effect of two the most important parameters on the response of the system, we are going to implement the new model of resistance inside the HEMPP to predict the dynamic stiffness and phase of the hydraulic engine mount. Figures (5-16), (5-17), (5-18) and (5-19) illustrate the comparison of the new model with

the old model along with the experimental results achieved by the Cooper Standard Company.

Here, 1mm and 2mm amplitude excitations have been performed. As observed, the frequency response of dynamic stiffness and phase of the system show great improvement. The model resistance agrees well with the experimental results, verifying the mechanical fluid equations that were derived and discussed in chapter 4. Figures (5-16) and (5-18) are showing dynamic stiffness is predicted well compared to the prediction of older version of HEMPP, not in magnitude, but also in frequency. Resonance for both prediction of dynamic stiffness by new version of HEMPP and experimental results happen at same frequency of 15 Hz, while the prediction by older version of HEMPP is showing that resonance happens at frequency of 20 Hz. By looking at these graphs, it is obtained that using the new model resistance in HEMPP, which is frequency dependent, improves the prediction of dynamic stiffness compared to the old version with resistance as a constant amount.

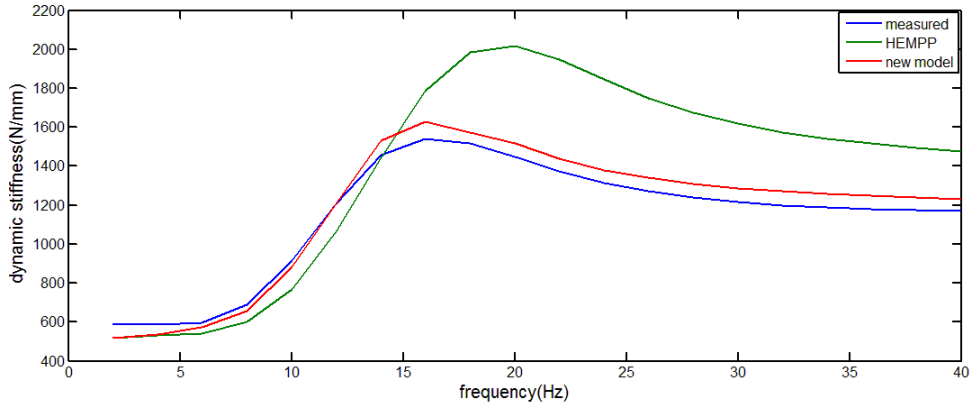

Figure 5-16: Frequency response of dynamic stiffness for 1 mm amplitude of excitation

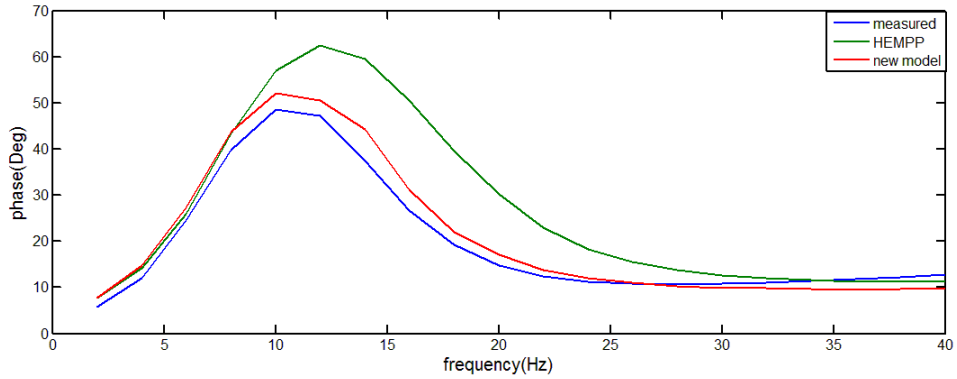

Figure 5-17: Phase vs. frequency of engine mount for 1 mm amplitude of excitation

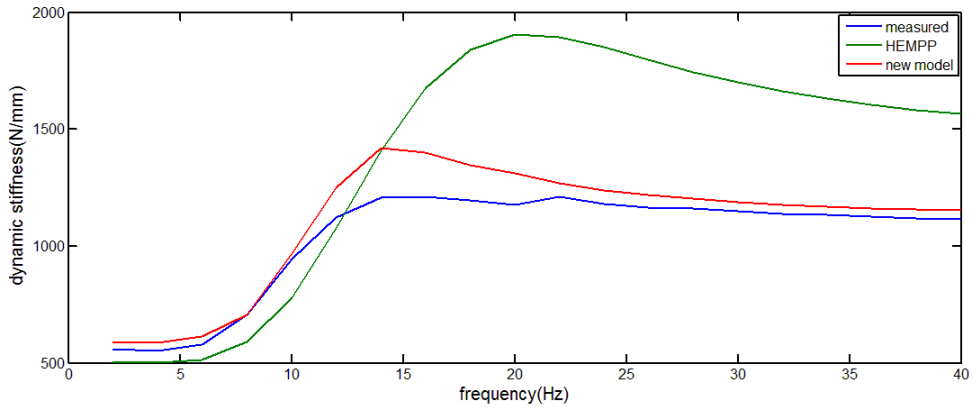

Figure 5-18: Frequency response of dynamic stiffness for 2 mm amplitude of excitation

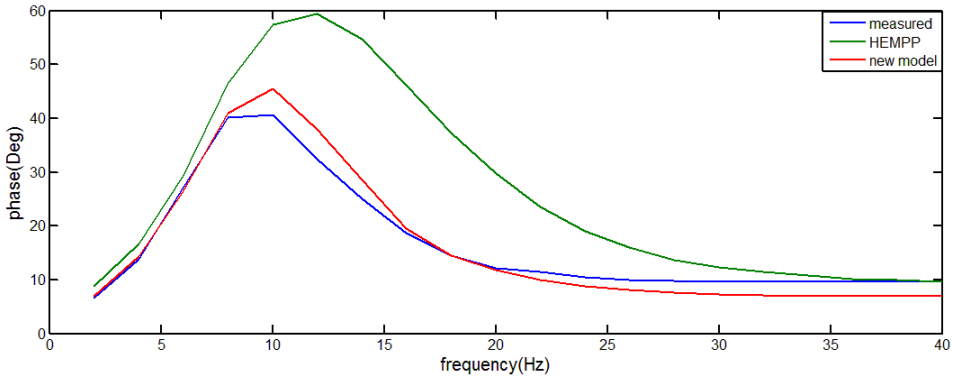

Figure 5-19: Phase vs. frequency of engine mount for 2 mm amplitude of excitation

6. Conclusion and recommendations

Modifying the prediction program of a hydraulic engine mount, HEMPP, was the main goal of this thesis. Different types of hydraulic engine mounts and their functionality have been discussed. It has been shown that development of the prediction program cannot be achieved unless the resistance of fluid inside the inertia track has been modeled accurately. The mechanics and characteristics of fluid under frequency and pulsatile excitation have been investigated in details. It is noteworthy that reciprocating motion of fluid inside inertia track complicates problem. For instance, Reynolds number is varying from 0 to the higher amount and then, when the direction of flow changes, the Reynolds number returns to zero and starts to increase depending on the frequency of excitation, which makes it difficult to predict the regime of flow. To solve the problem, the kinetic Reynolds number and the Womersley number have been used and studied to understand the attitude of the fluid flows inside inertia track. It was found that the regime of fluid depends on kinetic Reynolds number and dimensionless amplitude of excitation which in our case of study, flow is turbulent except at very low frequencies. Two test apparatuses have been assembled to investigate the characteristics of fluid inside pipes with different dimensions and also the frequency responses of pressure differentiation in a circular pipe when fluid passes through it under pulsatile and sinusoidal excitation.

Pipes with different cross sectional areas, interior roughness and rotational angles have been studied. The effect of changing the amplitude of excitation when fluid is moving under pulsatile excitation has also been experienced and discussed with the help of the first test apparatus. Using the second test setup, we were able to validate the new model of resistance for the fluid inside the inertia track of the engine mount. By implementing the new model of resistance inside the HEMPP codes written to predict the dynamic stiffness of the hydraulic engine mount, we could check the improvement of the closeness of experimental results and simulation data. The last step confirmed that

the new model for resistance is a reliable model, especially at lower frequencies of motion when only the inertia track has been chosen by fluid as a passage and the decoupler is excluded from the process.

It is recommended to investigate all other specifications and components of the engine mount, such as the main rubber and decoupler with upgraded methods. Modelling the main rubber under frequency excitation is one of the issues manufactures are always dealing with. Moreover, in the second test apparatus, to get more precise data, it is suggested to put another pressure sensor in the upper chamber near the end of the inertia track. It would help to observe the pressure at the end of the pipe and have a better understanding of the pressure drop of fluid inside the inertia track. Modelling the attitude of pulsatile flow inside the inertia track with help of upgraded software of computational fluid dynamics beside the mathematical model and experiments would improve modelling the resistance of the inertia track significantly. Improving test setup and its facilities and making them better able to provide a wider range of frequencies and amplitudes of excitation are other factors to be considered in future work.

References

[1] M. F.Golnaraghi and G. Nakhaie Jazar, "Development and Analysis of a Simplified Nonlinear Model of a Hydraulic Engine Mount", *Journal of Vibration and Control*, pp. 495-526, 2001

[2] G. Nakhaie Jazar and M. Farid Golnaraghi, "Nonlinear Modeling, Experimental Verification, and Theoretical Analysis of a Hydraulic Engine Mount", J*ournal of Vibration and Control*, 8; pp. 87-116, 2002

[3] C.E.Spiekermann, C.J. Radclie, E.D. Goodman, "Optimal design and simulation of vibrational isolation systems", *J. Mechanism, Transmissions, and Automation in Design*, pp. 271-276, 1985

[4] T.J. Royston, R. Singh, "Periodic response of nonlinear engine mounting systems". *SAE Technical Paper 951297,* 1995

[5] H.C. Lord, "Vibration dampening mounting", *US Patent 1,778,503*, 14 October 1930.

[6] W.D. Kim, H.J. Lee, J.Y. Kim, S.-K. Koh, "Fatigue life estimation of an engine rubber mount", *International Journal of Fatigue*, pp.553–560, 2004

[7] Yunhe Yu, N. G. (2001). "A literature review of automotive vehicle engine mounting. Mechanism and Machine Theory", pp. 123-142, 1999

[8] Siamak Arzanpour, "Active and semi-active bushing design for variable displacement engine", PhD thesis, University of Waterloo, Ontario, Canada, 2006

[9] Tian Ran Lin, Nabil H. Farag, Jie Pan, "Evaluation of frequency dependent rubber mount stiffness and damping by impact test", *Applied Acoustics* 66, pp. 829–844, 2005

[10] D.A. Swanson, "Active engine mounts for vehicles", *SAE Technical Paper 932432,* 1993

[11] R.H. Marjoram, "Pressurized hydraulic mounts for improved isolation of vehicle cabs", *SAE Technical Paper852349*, 1985

[12] M. Bemuchon, "A new generation of engine mounts", *SAE Technical Paper840259*, 1984

[13] P.E. Corcoran, G.H. Ticks, "Hydraulic engine mount characteristics", *SAE Technical Paper840407*, 1984

[14] W.C. Flower, "Understanding hydraulic mounts for improved vehicle noise, vibration and ride qualities", *SAE Technical Paper850975*, 1985

[15] T. Ushijima, K. Takano, H. Kojima, "High performance hydraulic mount for improving vehicle noise and vibration". *SAE Technical Paper880073,* 1988

[16] G. Kim and R. Singh, "A Study Of Passive And Adaptive Hydraulic Engine Mount Systems With Emphasis On Non-Linear Characteristics", *Journal of Sound and Vibration*",179,pp. 427_453, 1995

[17] A. Geisberger," Hydraulic engine mount modeling, parameter identification and experimental validation",M.A.Sc. Thesis, University of Waterloo, Ontario, Canada.2000

[18] Makhult, M., "Machine Support Design Based on Vibration Calculus",*AkademiaKiado*, Budapest 1977.

[19] R. Singh, G. Kim and P. V. Ravinder, "Linear analysis of automotive hydro-mechanical mount with emphasis on decoupler characteristics", *Journal of Sound and Vibration* 152(2), pp. 219-243, 1992

[20] L. Wang, J. Wang, I. Hagiwara, "An integrated characteristic simulation method for hydraulically damped rubber mount of vehicle engine", *Journal of Sound and Vibration* 286,pp. 673–696, 2005

[21] Frank M. White, Fluid mechanics, 1984

[22] Daniel J. Inman, engineering vibration, 3rd edition, 2007

[23] Wen-Bin Shangguan, Zhen-Hua Lu, "Modelling of a hydraulic engine mount with fluid–structure interaction finite element analysis", *Journal of Sound and Vibration 275,* pp. 193–221, 2004

[24] Wen-Bin Shangguan and Zhen-Hua LU, "Dynamic Characteristic Analysis of a Hydraulic Engine Mount With Lumped Model Based on Finite Element Analysis", *Noise and Vibration Conference and exhibition, Traverse city, Michigan*, 2003

[25] Wen-Bin Shangguan and Zhen-Hua LU, "Experimental study and simulation of a hydraulic engine mount with fully coupled fluid–structure interaction finite element analysis model", *Computers and Structures 82*, pp. 1751–1771, 2004

[26] Lirng Wang, Zhenhua LU and Ichiro Hagiwara, "Hydrostatic Fluid-structure Characteristic Analysis of Hydraulically Damped Rubber Mount", *World Congress on Engineering*, 2009

[27] Song He and Rajendra Singh, "Prediction of High Frequency Response characteristics of Hydraulic Mounts", *SAE Technical Paper2005-01-2410*, 2005

[28] R. Shoureshi, P.L. Graf, T.L. Houston, "Adaptive engine mounts", S*AE Technical Paper860549*, 1986

[29] Seung-Bok Choi and Young-Tai Choi**, "**Sliding Mode Control of a Shear-Mode Type ER Engine Mount", *KSME International Journal*, Vol. 13, No. I, pp. 26-33, 1999

[30] H. Mansour, S. Arzanpour, M. F. Golnaraghi, A. M. Parameswaran, "Semi-active engine mount design using auxiliary magneto-rheological fluid compliance chamber", *Vehicle System Dynamics,* Vol. 49, No. 3, pp. 449–462, March 2011

[31] Mahmoud S. Foumani, Amir Khajepour, and Mohammad Durali, "A New High-Performance Adaptive Engine Mount", *Journal of Vibration and Control*, Vol. 10, pp. 39-45, 2004.

[32] Dyke, S. J., Spencer, Jr B. F., Sain, M. K., Carlson J. D., "An Experimental Study of MR Dampers for Seismic Protection*", Smart Materials and Structures*, pp. 693-703, 1998

[33] Rabinow, J., "The Magnetic Fluid Clutch*", AIEE Transactions*, Vol. 67, pp. 1308–1315., 1948

[34] Peel, D. J., Stanway, R., and Bullough, W. A., "Dynamic Modelling of an ER Vibration Damper for Vehicle Suspension Applications*", Journal of Smart Materials and Structures,* no. 5, pp. 591-606, 1996

[35] Jolly, M. R., Bender J. W., Carlson J. D., "Properties and Application of Commercial Magnetorheological Fluids*", Journal of Intelligent Material Systems and Structures*, pp. 5-13, 1999

[36] Davis, L. C., "Model of Magnetorheological Elastomers*", Journal of Applied Physics*, 85(6), pp. 3348-3351, 1999

[37] Williams, E.W., Rigby, S.G., Sproston, J.L., Stanway, R., "Electrorheological fluids applied to an automotive engine mount", *Journal of Non-Newtonian Fluid Mechanics*, 47, pp. 221-238, 1993

[38] Golnaraghi, M.F., "Regulation of Flexible Structure via Nonlinear coupling*", Dynamic and Control 1*, pp. 405-428, 1991,

[39] T. Ushijima, S. Kumakawa, "Active engine mount with piezo-actuator for vibration control", *SAE Technical Paper930201,* 1993

[40] P.M.T Fursdon, A.J. Harrison, and D.P. Stoten, "The design and development of

a self-tuning active engine mount", *IMechE2000 Conference Transaction*, pp. 21-32, 2000

[41] S. Arzanpour, M. F. Golnaraghi, "Development of a bushing with an active compliance chamber for variable displacement engines", *Vehicle System Dynamics: International Journal of Vehicle Mechanics and Mobility*, Vol. 46 no. 10, pp. 867-887, 2008

[42] Yun-qing Zhang, Wen-bin Shangguan, "A novel approach for lower frequency performance design of hydraulic engine mounts", *Computers and Structures 84,* pp. 572–584, 2006

[43] S. He, R. Singh, "Estimation of amplitude and frequency dependent parameters of hydraulic engine mount given limited dynamic stiffness measurements", *Noise Control Engineering Journal* 53 (6), pp. 271–285, 2005

[44] Frank M. White, Viscous fluid flow (second edition), 2005

[45] J. R. WOMERSLEY, "Method for the calculation of velocity, rate of flow and viscous drag in arteries when the pressure gradient is known", *J. Physiol*. 127, pp. 553-563, I955

[46] Lewis F. Moody, "Friction factor for pipe flow". 1994

[47] H. Ockendon, J.R. Ockendon, "Viscose fluid", University of Oxford, 1995

[48] Colebrook, C. F. and White, C. M. "Experiments with Fluid Friction in Roughened Pipes". *Proceedings of the Royal Society of London. Series A, Mathematical and Physical Sciences*161 (906), pp. 367–381, 1937

[49] L-R Wang, Z-H Lu, I Hagiwara, "Finite element simulation of the static characteristics of a vehicle rubber mount", *Journal of Automobile Engineering,* Vol. 216 no. 12, pp. 965-973, December 1, 2002

[50] T. Sexl, "Uber den von entdeckten Annulare effekt", *Zeitschriftfuer Physik* 61, pp. 349-362, 1930

[51] T. S. Zhao and P. Cheng, "The friction coefficient of a fully-developed laminar reciprocating flow in a circular pipe", *Int. J. Heat and Fluid Flow*, Vol. 17, pp. 167-172, 1996

[52] Shigeo Uchida, "The Pulsating Viscous Flow Superposed on the Steady Laminar Motion of Incompressible Fluid in a Circular Pipe", 1956

[53] T. S. Zhao and P. Cheng, "A Numerical Study of Laminar Reciprocating Flow in a Pipe of Finite Length", *Applied Scientific Research,* Vol. 59 (1), pp. 11-25, 1998

[54] T.S. Zhao and P.Cheng, "Experimental studies on the onset of turbulence and frictional losses in an oscillatory turbulent pipe flow", *Journal of heat and Fluid Flow17*, pp. 356-362, 1996

[55] Winslow, W. M., "Induced Fibration of Suspensions", *Journal of Applied Physics*, Vol. 20, pp. 1137–1140, 1949

[56] Tuer, K. L., Golnaraghi, M. F., Wang, D., "Development of a Generalized Active Vibration Suspension Strategy for a Cantilever Beam Using Internal Resonance", *Nonlinear Dynamics* 5, pp. 131-151, 1994

[57] H. Mansour, S. Arzanpour, M. F. Golnaraghi, "Design of a solenoid valve based active engine mount". *Journal of vibration and control*, 2011

[58] Taylor, D. R. and Aghili, H., "An Investigation of Oscillating Flow in Tubes", *19th Intersociety Energy Conversion Engineering Conference*, *Proceedings of IECEC*, paper# 84916, pp. 2033-2036, 1984

[59] T. E. Moschandreou, C. G. Ellis, and D. Goldman, "Mass Transfer in a Rigid Tube with Pulsatile Flow and Constant Wall Concentration", *J Fluids Eng*., 132(8): 081202, 2010

[60] A Masih Hosseini, Siamak Arzanpour, Farid Golnaraghi and Ash M Parameswaran, "Solenoid actuator design and modeling with application in engine vibration isolator", *Journal of Vibration and Control*, March 2012

[61] RaffaellaTuzi and Paolo Blondeaux, "Intermittent turbulence in a pulsating pipe flow", *Proceedings of the World Congress on Engineering*, Vol. II WCE, July 1 - 3, 2009, London, U.K.

[62] Pu-zhenGao, Ting-hao Liu, Ting Yang and Si-chao Tan, "Pressure Drop Fluctuations in Periodically Fluctuating Pipe Flow", *J. Marine Sci. Appl.* 9, pp. 317-322, 2010

[63] A. Sarafrazian, M.F.Golnaraghi, S. Arzanpourand G. Behfarshad, "Model Based Virtual Prototyping for Hydraulic Passive Engine Mount with an Emphasis on Inertia Track", *Journal of Sound and Vibration,* 2013

[64] L-R Wang, J-C Wang, Z-H Lu, and I Hagiwara, "Investigation into the fluid-structure interaction of a hydraulically damped rubber mount on the basis of finite element analysis", *J. Automobile Engineering ,*Vol. 223 Part D, 2008

[65] R. Aris, "On the dispersion of solute in pulsating flow through a tube", *Mathematical and Physical Sciences*, Vol. 259, No. 1298, pp. 370-376, Dec. 29, 1960

[66] Edward L. Yellin, "Laminar-Turbulent Transition Process in pulsatile Flow", *Circulation research*, Vol. XIX, October 1966

[67] J. Y. Lin, J. M. Tarbel, "An experimental and numerical study of periodic flow in a curved tube", *Journal of Fluid Mechanic*, Vol. 100, part 3, pp. 623-638,1980

[68] Zhen-Hua LU and Wen-Bin Shangguan, "Dynamic characteristic analysis of hydraulically damped rubber mount: LP model based on Fsi Fe simulation", *Journal of Mechanical Strength*,2004

[69] L-R Wang, J-C Wang, Z-H Lu, and I Hagiwara, "Finite element-based parameter estimations for a characteristic simulation model of a hydraulically damped rubber mount for vehicle engines", *J. Automobile Engineering,* Vol. 221, 2007

[70] S. Arzanpour and M.F. Golnaraghi, "A Novel Semi-active Magnetorheological Bushing Design for Variable Displacement Engines", *Journal of Intelligent Material Systems and Structures* 19, 2008